HHS Public Access

Author manuscript

Nat Immunol. Author manuscript; available in PMC 2021 November 24.

Published in final edited form as:

Nat Immunol. 2021 June ; 22(6): 757–768. doi:10.1038/s41590-021-00926-0.

Dynamic regulation of B cell Complement Signaling is Integral to Germinal Center Responses

Arun Cumpelik[1,2], **David Heja**[1,2,‡], **Yuan Hu**[1,2], **Gabriele Varano**[3,‡], **Farideh Ordikhani**[1,2,4], **Mark P. Roberto**[3,6], **Zhengxiang He**[5], **Dirk Homann**[5], **Sergio A. Lira**[5], **David Dominguez-Sola**[3,4,5,7,†], **Peter S. Heeger**[1,2,5,†]

[1]Renal Division, Department of Medicine, Icahn School of Medicine at Mount Sinai, New York, NY

[2]Translational Transplant Research Center, Icahn School of Medicine at Mount Sinai, New York, NY

[3]Department of Oncological Sciences, Icahn School of Medicine at Mount Sinai, New York, NY

[4]Tisch Cancer Institute, Icahn School of Medicine at Mount Sinai, New York, NY

[5]Precision Immunology Institute, Icahn School of Medicine at Mount Sinai, New York, NY

[6]Graduate School of Biomedical Sciences, Icahn School of Medicine at Mount Sinai, New York, NY

[7]Department of Pathology, Icahn School of Medicine at Mount Sinai, New York, New York, USA.

Abstract

B cell maturation within germinal centers (GCs) generates diversified B cell pools and high-affinity B cell antigen receptors (BCRs) for pathogen clearance. Increased receptor affinity is achieved by iterative cycles of T cell-dependent, affinity-based B cell positive selection and clonal expansion by incompletely understood mechanisms. Here, we found that as part of a physiologic program, GC B cells repressed expression of decay-accelerating factor (DAF/CD55) and other complement C3-convertase regulators via Bcl-6, but increased C5b-9 inhibitor (CD59) expression. These changes permitted C3 cleavage on GC B cell surfaces, without membrane attack complex formation, and activated C3a-receptor and C5a-receptor signals required for positive selection.

Address correspondence to: Peter S Heeger, MD, Translational Transplant Research Center, Icahn School of Medicine at Mount Sinai, New York, USA; peter.heeger@mssm.edu, Phone: 212 241 6324; Fax: 212 987 0389, Or, David Dominguez-Sola, MD, PhD, Department of Oncological Sciences, Icahn School of Medicine at Mount Sinai, New York, USA; david.dominguez-sola@mssm.edu, Phone 212 824-8432; Fax: 646-537-9567.

‡Present addresses: Gabriele Varano: Department of Translational Medicine, Laboratory for Advanced Therapy Technologies (LTTA), University of Ferrara, Ferrara, Italy, David Heja: eGenesis Inc. Cambridge Massachusetts, USA

†These authors jointly supervised this work

Author contributions: A.C. contributed to the study design, performed the majority of in vivo and in vitro studies, prepared figures, wrote and edited the manuscript. D.H. and Z.H designed and prepared the DAF-TM targeting construct and performed in vitro characterization of the DAF-TM gene product in founder mice. Y.H and G.V. performed the studies on DAF gene regulation by BCL-6 experiments, BCR sequencing and together with M.P.R. performed RNA-Seq analyses, as well as reviewed and edited the manuscript. F.O. performed experiments including all studies with B1-8^{hi} mice and reviewed and edited the manuscript. D.H. and S.L. outlined the strategy for DAF-TM generation, served as critical reviewers of data and edited the manuscript. D.D-S. and P.S.H. conceptualized, designed and supervised the project, reviewed all data, wrote and edited the manuscript and provided funding.

Competing interests. The authors declare no competing interests.

Genetic disruption of this pathway in antigen-activated B cells, by conditional transgenic DAF overexpression or deletion of C3a and C5a receptors, limited mTOR activity in response to BCR-CD40 signaling, causing premature GC collapse and impaired affinity maturation. These results reveal that coordinated shifts in complement regulation within the GC provide crucial signals underlying GC B cell positive selection.

INTRODUCTION

Effective humoral responses to exogenous pathogens or vaccines depend on the generation of high affinity antibodies by affinity maturation. This key process is accomplished in germinal centers (GCs), specialized compartments within secondary lymphoid organs[1, 2] where B cells undergo iterative cycles of immunoglobulin gene somatic hypermutation, affinity-driven positive selection and clonal expansion[2]. Positive selection is triggered by enhanced B cell access to costimulatory signals from recruited follicular helper T cells (T_{FH}), upon antigen capture and presentation[2, 3, 4]. These signals determine the fate of GC B cells (survival and proliferation vs. cell death or differentiation) and are critical for sustaining the GC reaction and its immunological outputs[2, 5].

The precise molecular signals that drive positive selection and promote survival/expansion of selected GC B cells remain incompletely understood[2]. Previous studies showed that positive selection involves activation of PI3K/AKT and mTOR signaling, as well as MYC expression[2, 3, 6, 7]. While synergistic activation of CD40 and the B cell receptor (BCR) initiates triggering of a subset of these signals[4], integration of additional, unidentified ‘help’ cues is thought to actively contribute to successful selection[2]. Building upon previous work linking complement activation to adaptive T cell responses[8, 9, 10, 11] and the observation that GC B cells specifically lack surface expression of the complement regulator *Decay-Accelerating Factor* (DAF/CD55), we decided to investigate the notion that complement-initiated signaling impacts GC fate and function.

DAF is a glycophosphatidylinositol-(GPI)-anchored, complement system regulator that functions only on DAF-expressing cell surfaces[12]. DAF accelerates the decay of multimeric C3 convertases, limiting the amplification/progression of the complement cascade, and preventing formation of C3- and C5-cleavage products C3a and C5a[12]. It is encoded within the Regulators of Complement Activation (RCA) syntenic region of human chromosome 1, which includes *Cr1* (CD35), *Cr2* (CD21), C4b-binding protein (*C4BP*), and human membrane co-factor protein (*MCP/Cd46*)[13]. In mice, chromosome 1 encodes a differently arranged but syntenic region for homologues of *DAF/Cd55*, *Cr2*, *C4bp* and *Cr1l* (*Crry*, absent in humans)[14]. These regulators collectively dissociate C3 convertases and/or facilitate inactivation of C3b to iC3b. Herein we demonstrate that reprogramming of surface complement regulator expression in GC B cells by BCL-6 enables local C3a/C5a-receptor signaling and optimal mTOR activation required for positive selection and GC homeostasis.

RESULTS

Coordinated shifts in complement regulators on GC B cells

We initially observed that DAF is highly expressed on IgD^+ B cells, but undetectable on $GL7^+$ B cells in the spleen of 4-hydroxy-3-nitrophenyl-acetyl-Keyhole-Limpet Hemocyanin (NP-KLH) immunized mice (d10, Fig 1a). Flow cytometric analyses confirmed high DAF surface expression on naïve murine ($B220^+IgD^+$) and human ($CD19^+IgD^+CD38^{lo}$) B cells (Fig 1b–c, Extended data Fig 1a–b). DAF expression on murine IgD^{--} GC B cells, defined by expression of the markers GL7 and Fas, and on human IgD^- GC B cells, defined by expression of the surface markers CD38 and CD10, is >10-fold lower compared to naïve B cells. DAF expression recovers in murine ($IgD^-GL7^-Fas^-CD38^+$) and human memory ($CD19^+IgD^-CD27^+$) B cells. In immunized mice, DAF downregulation on GC B cells was evident by day 6 after immunization (MFI 5030±300.2, n=4), decreased further on day 8 (MFI 1753±26.66, n=4, $p<0.001$ vs d6, unpaired t test) to a minimum level on day 10 (MFI 560.5±63.58, n=4, $p<0.001$ vs d6 and d8, unpaired t test), and maintained through day 12 (MFI 516.8±65.22, n=4, not significant vs d10, unpaired t test). DAF downregulation was commensurate in ($CD86^{hi}CXCR4^{lo}$) light zone, ($CD86^{lo}CXCR4^{hi}$) dark zone and grey zone[15] ($CD86^{hi}CXCR4^{hi}$) GC B cells (Extended data Fig 1c). Analysis of other RCA proteins showed lower Cr1/Cr2 on murine GC B cells and very low to absent *Crry* expression in all B cell subsets (Fig 1d, Extended data Fig 1b). Human GC B cells also expressed consistently lower levels of CD46, CR1 and CR2 (Fig 1c, Extended data Fig 1e). We observed, reciprocal changes in mRNA expression of human and syntenic murine RCA genes in GC- and naive B cells (Fig 1d–e, Extended data Fig 1f). In contrast to RCA members, murine and human GC B cells expressed higher levels of the membrane attack complex (MAC) inhibitor CD59 (protectin, encoded outside the RCA, Fig 1b–c, Extended data Fig 1d–e). Both murine and human GC B cells stained positive for the C3 cleavage product C3b (Fig 1f, Extended data Fig 1g) and GCs in human tonsil tissue sections stained positive for C3b, C5b, and C6, but not C9 (Fig 1g, Extended data Fig 1h), reflecting the functional absence of C3-convertase regulation but presence of CD59 activity. Together, these results demonstrate that the coordinated and dynamic reorganization of complement regulatory proteins facilitates C3 convertase activity on GC B cells, while blocking MAC formation (Extended data Fig 2a, **schematic**).

BCL-6 represses DAF expression in GC B cells

The transcription factor Bcl-6 is required for GC B cell generation and is expressed in committed $GL7^+CCR6^+CD38^+$ B cells[5] prior to GC entry (day 3–4 post-immunization)[16, 17]. To further delineate the kinetics of DAF downregulation in GC B cells, we immunized Bcl-6-YFP reporter mice[17] and 3 days later analyzed DAF and Bcl-6 protein expression (BCL-6-YFP) on IgD^-GL7^+ B cells (Fig 2a, Extended data Fig 2b). These analyses showed that on d3 (prior to GC formation/coalescence), Bcl-6-YFP^+ B cells already lacked DAF expression, coinciding with the upregulation of Bcl-6 expression during early GC-commitment.

Analysis of available gene expression data on human GC-derived B cell lymphoma and multiple myeloma cell lines confirmed the inverse correlation of *DAF* and *BCL-6* expression

(Extended data Fig 2c). BCL-6 is a major transcriptional repressor in GC B cells[16], and based on available human GC B cell ChIP-Seq data[18], it is significantly enriched at an active 5' proximal regulatory region and an intronic enhancer in the *Cd55* gene (defined by the distribution of H3K4Me1 and H3K4Me3 histone marks; Fig 2b), suggesting that BCL-6 could directly modulate DAF expression. We further noted BCL-6 enrichment at multiple regulatory regions throughout the RCA (including 5' regulatory regions of *CD21, CR1/2, C4bBP-CD46*), but notably absent from regulatory regions upstream of CD59 (Extended data Fig 2d–e). Consistent with these observations, transient BCL-6 overexpression in KMS27 cells (multiple myeloma cell line, BCL-6^{-}DAF^{+}) reduced surface DAF and CD46 expression without altering CD59 expression (Fig 2c–d). Conversely, overexpression of a dominant negative BCL-6 mutant[19] (BCL-6-ZF, Fig 2e–f) in SUDHL5 B cell lymphoma cells (BCL-6^{hi}DAF^{lo}) increased surface DAF and CD46 expression, without altering CD59. Similarly, BCL-6 inactivation by a small-molecule BCL-6 inhibitor[20] (FX-1) increased DAF (5/5 lymphoma lines tested) and CD46 expression (2/4 lines increased, 2/4 no change) (Fig 2g–h). CD59 expression was also increased in these conditions (Fig 2i, 3/3 lines tested). Finally, transient BCL-6 overexpression in TOLEDO B cells (B cell lymphoma, BCL-6^{lo}DAF^{hi}), but not that of two truncated, transcriptionally inactive BCL-6 variants[19], repressed luciferase reporter activity driven by the two regulatory regions identified in the *Cd55* gene (Fig 2j). Thus, BCL-6 is a direct transcriptional repressor of *DAF* gene expression in GC B cells.

GC homeostasis requires GC B cell C3aR1/C5aR1 signaling

To investigate the functional relevance of DAF downregulation in GC B cells, we engineered mice expressing a conditional (Cre-lox), transmembrane domain-containing, transgenic form of DAF (DAF-TM, Extended data Fig 3a), and intercrossed these mice with B cell-specific *CD19*-Cre[21] or *Cγ1*-Cre mice[22]. While *CD19*-Cre is active throughout B cell development[21], *Cγ1*-Cre mediated recombination is restricted to GL7^{hi}Fas^{hi} GC B cells early after immunization (25–50% at d4) and is maximum (75–90%) at the peak of the GC reaction[22] (d10–14). Using B cells isolated from *DAF-TM*$^{+/+}$x*CD19*-Cre$^{+/-}$ mice, we confirmed expression of a non-cleavable, DAF-TM protein on GC B cell surfaces that functionally limits C3b deposition (Extended data Fig 3b–d). Control analyses showed GPI-anchored CD59 is cleaved from the same GC B cells (Extended data Fig 3e–f). Consistent with published kinetics of *Cγ1*-Cre activity[22], sequential analyses of GL7^{+}Fas^{+} GC B cells from immunized *DAF-TM*$^{+/+}$*xCγ1*-Cre$^{+/-}$ (DAF-TM^{Cγ1}) mice showed expression of non-cleavable, functional DAF-TM protein as early as d4 (~30% of GC B cells) peaking by d10 post immunization with NP-KLH (>90% of GC B cells; Extended data Fig 4a). We also observed detectable DAF-TM expression on ~10% of activated GL7^{+}CCR6^{+}CD38^{+} B cells[5] on d4, increasing to 75% by d10 (Extended data Fig 4a). On d10–12 we observed 2–3-fold higher DAF expression on DAF-TM^{Cγ1} GC B cells vs. Cre$^{+/-}$ controls (Fig 3a), without alterations in expression levels of CD59, CR1/2, or *Crry* among naïve, GC and memory B cells (blue, Extended data Fig 4b–d).

Flow cytometry analyses of DAF-TM^{Cγ1} mice immunized with NP-KLH (Fig 3b–e black vs. blue) or sheep red blood cells (SRBC, Extended data Fig 4e–g) showed significantly lower relative and absolute frequencies of splenic GC B cells (~3-fold; $p<0.001$). GCs

induced upon NP-KLH (Fig 3d–e) and SRBC immunization (Extended data Fig 4g) initially formed (d4–8) and adequately polarized (Extended data Fig 4h), but did not continue to expand beyond day 8–10 (coinciding with the peak of DAF-TM transgene expression). NP-KLH-induced GCs prematurely collapsed by day 12 (Fig 3d–e), associated with significantly reduced numbers of memory and plasma cells (Fig 3f, Extended data Fig 4i–k), together demonstrating disruption of GC function/maintenance.

The absence of DAF expression on GC B cells would be expected to lift restraint on cell surface C3 convertase formation, resulting in augmented release of C3a and C5a anaphylatoxins[8, 9, 23] (Extended data Fig 2a) and subsequent signaling through their respective receptors. These receptors (C3aR1 and C5aR1) are upregulated on murine and human GC B cells (Extended data Fig 5a–d), along with C5aR2/C5L2, an alternative "decoy" receptor for C5a [24] (Supp Fig 5e). Indeed, GC responses in newly generated *C3ar1*$^{fl/fl}$*C5ar1*$^{fl/fl}$x*Cγ1*-Cre$^{+/-}$ mice (Δ*C3ar1*/*C5ar1*^{Cγ1}) and in which C3aR1/C5aR1 are absent on GC B cells phenocopied those of the DAF-TM^{Cγ1} mice (Fig 3c–f, Extended data Fig 4e–h, Extended data Fig 5a–e), including reduced GC size on d10 (Extended data Fig 5f–g). Absence of either C3aR1 or C5aR1 showed an intermediate phenotype (Extended data Fig 4e–f). These defects in GC formation and maintenance in Δ*C3ar1*/*C5ar1*^{Cγ1} and DAF-TM^{Cγ1} mice associated with substantial reductions in the fraction of actively proliferating cells (Ki67 staining and EdU incorporation, Fig 3g–h) and with significant increases in active caspase 3 positivity (a bona-fide marker of cell death in GCs [25], Fig 3i–k). All these parameters indicate a severe disruption of GC homeostasis.

Studies with mice germline-deficient in complement components and C3$^{-/-}$ WT bone marrow chimeras indicated that compared to Δ*C3ar1*/*C5ar1*^{Cγ1} mice, CD21 (CR2) deficiency only modestly reduced GC formation in the setting of high antigen availability, consistent with previous observations[2, 26, 27] (Extended data Fig 6a–b). Optimal GC formation required systemic C3 as well as C1q, but not factor B or mannose binding lectin (MBL), the latter implicating the classical pathway of complement activation (Extended data Fig 6c).

The disruption of GC responses in DAF-TM^{Cγ1} and Δ*C3ar1*/*C5ar1*^{Cγ1} mice also associated with a pronounced defect in antibody generation, with 4–6-fold lower titers of total and high affinity anti-NP antibodies in NP-KLH-immunized mice ($p<0.001$, Fig 4a–b) and similarly reduced titers of anti-SRBC (Fig 4c) antibodies in SRBC-immunized mice. Together with the observed 4-fold fewer NP-reactive GC B cells ($p<0.01$, Fig 4d–e), the data suggest impaired affinity maturation. We thus quantified frequencies of BCR somatic mutations known to confer high affinity, sequencing the variable regions of the λ$^+$ BCRs in GC B cells of DAF-TM^{Cγ1}, Δ*C3ar1*/*C5ar1*^{Cγ1} and control mice immunized with NP-KLH (Fig 4f–g, Supplementary Table 1). DAF-TM^{Cγ1}, Δ*C3ar1*/*C5ar1*^{Cγ1} GC B cells carried ~2-fold fewer high affinity (W33L, K59R) BCR mutations in Vh186.2 immunoglobulin regions. The analysis of intronic sequences downstream of the J_{H4} gene, a region targeted by somatic hypermutation activity but not subject to selection[28], showed that DAF-TM^{Cγ1} and Δ*C3ar1*/*C5ar1*^{Cγ1} GC B cells had an overall lower frequency of somatic hypermutation (Fig 4h, Supplementary Table 1), suggesting that the reduction in affinity maturation in these mice is due to reduced cycling and hypermutation of these cells within GCs.

Competitive selection of GC B cells requires C3aR1/C5aR1

To gain further mechanistic insights into these defects, we performed RNA-seq on flow-sorted GL7^{+}Fas^{+} B cells at d10 post-SRBC immunization (at peak of DAF-TM expression, and GC size plateau in DAF-TM mice, Fig 3d–e, Extended data Fig 4g), sorting for DAF^{+} GC B cells in DAF-TM$^{C\gamma1}$ mice. Using supervised analysis, we identified ~85 differentially expressed genes between DAF-TM$^{C\gamma1}$ and control GC B cells (DESeq2, padj<0.05 cutoff) (Supplementary Table 2). Approximately two-thirds of these genes, including DAF, were upregulated in DAF-TM$^{C\gamma1}$ GC B cells and belonged to families of membrane-associated proteins and/or secreted molecules involved in cell-cell interactions, cell adhesion and/or chemokine-driven cell motility (Extended data Fig 7a, Supplementary Table 2). Among the downregulated genes, we found those encoding subunits of the PI3-K signaling complex (*Pik3cg, Pik3c2a*) and other proteins reportedly involved in the control of fatty acid and RNA metabolism (*Cdk19, Apobec1, Ptbp3, Insig1, Apoc2*) (Supplementary Table 2). A fraction of differentially expressed genes in DAF-TM$^{C\gamma1}$ GC B cells encoded proteins involved in immunoregulatory interactions and chemokine signaling with increased expression levels of *Ccr7, Ccl5, Ccl6, Tlr7, Sell (Cd62l) and S1pr1* (Fig 5a–b). Activated GL7^{+}Fas^{+} B cells at the T/B border or CCR6^{+}CD38^{+}GL7^{+}Fas^{+} pre-GC cells[5, 29] express many of these factors, which are typically downregulated as activated B cells enter and expand in the GC (*e.g., Ccr7, Tlr7, S1pr1, Sell/Cd62l*) [30, 31, 32, 33, 34]. Accordingly, GSEA detected significant enrichment for pre-GC gene signatures in DAF-TM$^{C\gamma1}$ GC B cells (Fig 5c). Flow cytometry analyses confirmed higher expression of *Ccr7, Tlr7, S1pr1* and *Sell/Cd62L* on GL7^{+}Fas^{+} B cells in DAF-TM$^{C\gamma1}$ and Δ*C3ar1*/*C5ar1*$^{C\gamma1}$ mice (Fig 5d, Extended data Fig 7b–c). We also found increasing frequencies of CCR6^{+}CD38^{+}GL7^{+}Fas^{+} B cells in DAF-TM$^{C\gamma1}$ and Δ*C3ar1*/*C5ar1*$^{C\gamma1}$ mice at d6–10 post-immunization (Fig 5e), suggesting the accumulation of B cells at transitional stages between naïve and GC B cell phenotypes[5, 29]. The IF analysis of splenic tissue sections (Extended data Fig 5g) showed that GL7^{+} cells were confined to GCs in both Δ*C3ar1*/*C5ar1*$^{C\gamma1}$ and control mice, and did not form clusters at the B-T border[35, 36].

To better understand these findings, we co-transferred equal numbers of BCR transgenic CD45.1/2 B18^{hi} xCγ1Cre$^{+/-}$ and CD45.2 B18^{hi} DAF-TM$^{C\gamma1}$ B cells into CD45.1 recipients. Adoptive transfer of congenic B1–8^{hi} transgenic B cells enabled specific and time-sequential, comparative analysis of cell fate between antigen-activated DAF-TM^{+} and control B cells in response to NP immunization. These experiments showed that CD45.2 B18^{hi} DAF-TM$^{C\gamma1}$ B cells failed to expand (Fig 5g–i), both in the extrafollicular compartment and particularly within GCs, as evidenced by higher CD45.1/2 vs CD45.2 ratios and higher competitive indices[37] (2–4-fold depletion, increasing from d5 to d9) (Fig 5i). In non-immunized mice, the ratios of CD45.1/.2 vs CD45.2 cells remained stable (1:1 post-transfer). We also observed a progressively increasing percentage of GL7^{+}Fas^{+} B cells co-expressing CCR6 and CD38 within DAF-TM^{+} vs control B18^{hi} cells (Fig 5j). Thus, DAF-TM B cells were initially activated in response to NP (confirmed by the upregulation of CCR6^{+}, CD62L^{+}, GL7^{+} and Fas^{+}) and could be recruited to GCs, but they (abnormally) retained early activation markers and were progressively outcompeted by wildtype B cells in all compartments. Collectively, these findings and the above noted alterations in B cell proliferation and cell death, suggest that absence of DAF and effective C3aR1/C5aR1

signaling are essential for optimal B cell expansion and competitive fitness during T-dependent antigen responses.

C3aR1/C5aR1 activate mTOR and MYC in GC B cells

GC entry and positive selection are driven by concurrent signals triggered by the BCR and ligand/receptor interactions offered by T_{FH} cells[2]. Co-activation of BCR and CD40 signaling initiates key survival pathways (e.g., mTOR, MYC) essential for positive selection in the light zone [3, 4] and activates E2F-dependent B cell expansion in the dark zone[38]. Consistent with these concepts, pathway analysis (GSEA) using a library of signatures defining general biological processes (HALLMARK and GO categories[39]) revealed a significant loss of gene sets related to MYC, mTOR, CD40 and E2F signaling, cellular proliferation and biosynthesis in DAF-TM$^{C\gamma1}$ GC B cells (Fig 6a, Extended data Fig 8a). These results implied that C3 convertase activity and C3aR1/C5aR1 signaling are also necessary for effective GC B cell activation in response to BCR/CD40 signals.

To test this concept, we immunized groups DAF-TM$^{C\gamma1}$, Δ*C3ar1*/*C5ar1*$^{C\gamma1}$ and control *Cγ1*-Cre$^{+/-}$ mice and 10 days later, analyzed MYC expression and mTOR activity (by phosphorylation of the S6 ribosomal protein, pS6) 4h after i.v. injection of either control IgG, anti-CD40, anti-IgM F(ab')$_2$ or anti-CD40+anti-IgM F(ab')$_2$ antibodies (see Extended data Fig 8b–d for controls). Anti-CD40+anti-IgM F(ab')$_2$ induced significant increases in pS6 (mTOR substrate) and MYC expression in WT GC B cells, with significantly reduced responses in DAF-TM$^{C\gamma1}$ and Δ*C3ar1*/*C5ar1*$^{C\gamma1}$ GC B cells (Fig 6b–c), despite comparable levels of CD40 and BCR (CD79, Igα/Igβ) expression among genotypes (Fig 6d–e). To test whether these differences were confounded by binding of anti-IgM F(ab')$_2$ to circulating IgM, we performed analogous experiments by transferring control or germline *C3ar1*$^{-/-}$*C5ar1*$^{-/-}$ B cells into IgM-deficient recipients (μMT^{-} mice,[40] Extended data Fig 8e–f). These assays confirmed that combined anti-CD40+anti-IgM F(ab')$_2$ treatment induced pS6 upregulation in control B cells but failed to do so efficiently in *C3ar1*$^{-/-}$*C5ar1*$^{-/-}$ B cells (ELISAs confirmed essentially absent serum IgM, Extended data Fig 8g).

Complementary *in vitro* experiments showed that addition of recombinant C3a/C5a effectively induced mTOR signaling in WT GC (and naïve) B cells exposed to CD40/IgM stimulation (Fig 6f–g) but had no measurable effect on *C3ar1/C5ar1*-deficient B cells. C3a/C5a alone induced low levels of S6 protein phosphorylation in naïve and GC B cells in absence of anti-CD40/IgM (Extended data Fig 8h).

DISCUSSION

The dynamic control of local complement activation accomplished via altering surface complement regulator expression levels represents an overlooked component of the GC gene program. Coordinated reprogramming of complement regulators on GC B cells allows enhanced C3a/C5a production and local B cell C3aR1/C5aR1 signaling, which directly contribute to B cell positive selection events required for GC formation, maintenance and function. Our data identify BCL-6 as a crucial transcriptional repressor involved in this process, although contribution by other transcriptional controllers is possible. Our

observations that a) DAF is essentially absent on GC B cells, and b) transgenic DAF overexpression markedly alters GC responses in the absence of compensatory changes in the expression of other key regulators (e.g., CR2, *Crry* or C5aR2) and c) CR2 signaling contributes little in this antigen rich setting[41] all suggest that BCL-6-induced repression of DAF is vital for optimal GC function. While we did not genetically assess the impact of other complement regulators, it is conceivable that coordinated repression of DAF, CD46 (human), and CD21/35 are all required to optimally initiate GC B cell C3aR1/C5ar1 signaling. The simultaneous upregulation of CD59 (BCL-6-independent) prevents MAC formation and likely inhibits B cell lysis despite upstream complement activation. CD59 upregulation on GC B cells likely contributes to GC B cell survival: others showed CD59-deficient mice develop weaker T-dependent antibody responses[42]. The positive effects of the FX-1 BCL-6 inhibitor on CD59 levels are possibly indirect (ChIP-seq showed no binding in regulatory regions).

Positive selection in GCs requires BCR activation and ligation of B cell CD40 along with signals initiated by cytokines and other ligands, e.g., ICOSL[2, 3, 4]. While these concurrent signals induce mTORC1 activation and MYC upregulation, their integration has remained incompletely understood. The finding that absent C3aR1/C5aR1 signaling in GC B cells results in severe defects in GC formation/maintenance and precludes effective activation of mTOR (and MYC expression), along with our previous studies linking C3aR1/C5aR1 to PI3-Kγ/AKT-dependent mTOR activation in other immune cells[9, 10], strongly suggest that complement receptor-initiated signals are rate limiting, and coalesce with other positive selection cues in B cells undergoing T cell-dependent positive selection. We surmise that the observed signaling defects during positive selection explain the major GC phenotypes in DAF-TM$^{C\gamma1}$ and Δ*C3ar1*/*C5ar1*$^{C\gamma1}$ mice, namely the competitive disadvantage, the alterations in proliferation/death balance, as well as the defects in GC formation, maintenance and loss of affinity.

A notable finding is that expression of DAF-TM or absence of B cell C3aR1/C5aR1 signaling resulted in the accumulation of GL7$^+$ Fas$^+$ B cells expressing CD62L, TLR7, S1P1, CCR7 and CCR6, both at the transcript and protein level. Upregulation of these markers in GL7$^+$ cells has been reported in antigen-activated B cells prior to GC entry[5, 29, 43] but also in memory B cell precursors (typically with low antigen affinities),[44] while being specifically downregulated in GC B cells. Thus, this surface phenotype precedes key cell fate transitions in mature B cells. Persistence of these markers in antigen-activated B cells from DAF-TM and C3aR1/C5aR1-null mice strongly suggests that, upon activation by antigen and T cells, these B cells are incapable of completing such fate transitions. Accordingly, the progressive depletion of DAF-TM and *C3ar1*$^{-/-}$*C5ar1*$^{-/-}$ B cells in competitive chimeras suggests that these cells will be eventually lost to more fit, wildtype B cells, thereby preventing their effective accumulation prior to GC entry (noting we did not find any pre-GC clusters in tissue sections) or as early memory B cell precursors (noting the overall numbers of definitive memory B cells are diminished).

The demonstration of an integral role for GC B cell-expressed DAF and C3aR1/C5aR1 signaling in the control of GC dynamics is distinct from other reported effects of complement in humoral immunity[45, 4611, 26]. Ligation of B cell-expressed CD21 (CR2) by

C3dg-coated antigen lowers naïve B cell activation thresholds, in part by phosphorylating CD19. This mechanism is most relevant for B cells responding to T-independent antigens, but not T-dependent responses, and in contrast to our observed >90% reduction in antigen-specific serum antibody in absence of C3aR1/C5aR1 signaling on B cells, CD21 deficiency only modestly reduces T cell-dependent humoral immune responses [41]. Other studies employing germline *C3ar1/C5ar1*-deficient animals showed that B cell-expressed C3aR1/C5aR1 signals drive early activation events (including upregulation of AID and BCL-6), but potential links to GC dynamics and GC-dependent affinity maturation were not addressed[46]. A recent 2021 paper [47] reported DAF downregulation on human GC B cells, largely confirming our findings. The authors suggested that DAF downregulation would enhance phagocytosis of GC B cells and could possibly also facilitate interaction with T cells; mechanisms that we did not directly test in our study but could directly/indirectly impact affinity maturation and positive selection in the GC [48, 49], contributing to the phenotypes that we detect in our models.

Key studies by Kemper and colleagues, among others, reported unanticipated roles for intracellular complement (i.e., the complosome) in physiological T cell immune responses, particularly in humans[50, 51]. Intracellular C3, C3a and C5a have been detected in human and murine B cells[46, 51, 52] and may contribute to early B cell activation[46] but we are not aware of any evidence that intracellular complement participates in GC responses. Our BM chimera studies indicate a dominant role for systemic C3 in the observed GC B cell effects, although we noticed a subtle (albeit significant) contribution of immune cell derived C3. The finding that GC responses are impaired in C1q-deficient, but not factor-B-deficient or MBL-deficient, mice adds further mechanistic insight into the unexplained observation that C1q/BCR ligations contribute to successful GC responses[53]: in the context of physiologically downregulated DAF on GC B cells, C1q crosslinking of surface IgM may initiate complement activation and subsequent C3aR1/C5aR1 signaling required for optimal positive selection. Of note, C1q transcripts are specifically upregulated in positively-selected, MYC^+ GC B cells[7], raising the possibility that this process could be dependent upon locally produced, rather than systemic, C1q.

Overall, our results support an enhanced view of complement signaling as an essential element of the humoral response; and indicate that the contribution of this signaling pathway to immunity is multifaceted, bridging pathways and regulatory modules involved in both innate and adaptive immune responses. Analyses of public databases show that aside from GC B cells, BCL-6 and DAF are also inversely expressed in DCs and neutrophils (Immgen.org), suggesting that coordinated repression of C3/C4 convertase regulators could enable local complement activation to modulate other immune cell functions, with significant implications beyond those regarding B cells. Our findings also identify unrecognized targets for therapeutic manipulation of humoral immunity in health and disease. Manipulation of complement signaling, particularly the complement regulator/C3aR1/C5aR1 axis here described, would facilitate the targeted modulation of adaptive immune responses in multiple settings: the design of vaccines, the management of transplants and, contextualizing our study with recent findings[54, 55], in the modulation of immune responses to cancer.

METHODS

Mice

C57BL/6/J (B6, cat# 000664), B6;129S4-*C3*^{tm1Crr}/J (*C3*^{tm1Crr}, C3$^{-/-}$, cat# 029661), B6.129P2(C)-*Cd19*$^{tm1(cre)Cgn}$/J (cat# 6785, *CD19*-Cre$^{+/-}$), C.129P2(Cg)-*Ighg1*$^{tm1(cre)Cgn}$/J (cat# 010611, *Cγ1*-Cre$^{+/-}$), B6.SJL-*Ptprc*^{a} *Pepc*^{b}/BoyJ (cat# 002014, CD45.1), B6.129S2-*Ighm*^{tm1Cgn}/J (cat# 002288, μMT) mice, all *H-2*^{b}, were purchased from Jackson Laboratory (Jax) and bred at the Icahn School of Medicine at Mount Sinai. Experiments using *CD19*-Cre$^{+/-}$ and *Cγ1*-Cre$^{+/-}$ knock-in models were performed using Cre$^{+/-}$ heterozygotes. Germline B6 *C3ar1*$^{-/-}$*C5ar1*$^{-/-}$ mice were generated as described[13,15].

The following animals were kind gifts: B6.129S4-*Mbl1*^{tm1Kata} *Mbl2*^{tm1Kata}/J (*mbl1*$^{-/-}$*mbl2*$^{-/-}$) from G. Stahl (Harvard Medical School), complement factor B$^{-/-}$ (fB) produced by M. Pekna (Gothenburg, Sweden) from M. Zhang (SUNY Downstate), *Cr1*$^{-/-}$ (CD21-deficient) produced by M Carroll (Harvard Medical School)[58] (SUNY Downstate), B6(Cg)-*C1qa*$^{tm1d(EUCOMM)Wtsi}$/TennJ (Jax cat# 031675, *C1q*$^{-/-}$) from B. Diamond (Feinstein Institute, Northwell Health) *and Bcl-6*^{YFP}mice[17] generated by T. Okada (Kyoto University, Kyoto, Japan), from S. Reiner, (Columbia University) and B18^{hi} BCR transgenic mice from M. Nussenzweig (Rockefeller University).

B6 *C5ar1*$^{fl/fl}$ mice were described previously[59]. B6 *C3ar1*$^{fl/fl}$ mice were generated from ES cells purchased from the EUCOMM consortium. The Mouse Genetics core facility at Icahn School of Medicine at Mount Sinai injected the *C3ar1*$^{fl/fl}$ ES cells into pseudo-pregnant B6 mice using standard techniques. After validating founder genotype, the animals were crossed to B6.129S4-*Gt(ROSA)26Sor*$^{tm2(FLP*)Sor}$/J mice (Jax cat# 012930) to remove the neo cassette. The *C5ar1*$^{fl/fl}$ and the *C3ar1*$^{fl/fl}$ animals were crossed to *Cγ1*-Cre transgenics to produce *C3ar1*$^{fl/fl}$x*Cγ1*-Cre$^{+/-}$ and *C5ar1*$^{fl/fl}$x*Cγ1*-Cre$^{+/-}$ mice and then intercrossed to produce *C3ar*$^{fl/fl}$/*C5ar1*$^{fl/fl}$x *Cγ1*-Cre$^{+/-}$ (Δ*C3ar1*/*C5ar1*^{Cγ1}) mice.

All animals were housed in the Center for Comparative Medicine and Surgery at the Icahn School of Medicine at Mount Sinai under Institutional Animal Care in accordance with guidelines of the Association for Assessment and Accreditation of Laboratory Animal Care International approval IACUC-2018–0014. Mice were housed in pathogen-free conditions, at 22°C and 30–70% humidity in a 12h light/dark cycle and provided ad libitum access to food and water. Experiments were performed in compliance with ethical guidelines under IACUC approval number 2018–0084 (approved 2/2018). Experiments with groups of age- (6–12 weeks) and sex-matched mice, using littermates or animals maintained in the same room and co-housed within the same cages for >2 weeks.

Generation of conditional DAF-TM transgenic mouse

The DAF-TM transgenic gene (Extended data Fig 3) was constructed using the coding sequence of the mouse *Daf1* gene (*Cd55*) containing the complement regulatory domain[60], replacing the signal sequence for glycophosphatidylinositol-(GPI)-anchor addition with that of the transmembrane helix domain of human tissue factor (non-signaling, see Extended data Fig 3). Transgene expression driven by the CAG promoter in the Rosa26 locus is regulated by a loxP flanked transcriptional stop element.

Paired Cas9^{D10A} nickase (Cas9n) was used to target the transgene into the *Rosa26* locus (targeting sequences (see Extended data Fig 3a for details): ACTGGAGTTGCAGATCACGA GGG, GGCAGGCTTAAAGGCTAACC TGG). The gRNA-A and gRNA-B sequences were inserted into two separate plasmid constructs on the pX460 (Addgene) backbone that each also contained a copy of the Cas9n coding sequence. A pUC57_DAF-TM homology repair plasmid was prepared comprising the DAF-TM transgenic construct flanked by Rosa26 homology arms. Purified plasmid DNA constructs from transformed *E. coli* (Invitrogen/ThermoFisher) using EndoFree Plasmid Maxi kit (Qiagen) were verified by sequencing, transferred into fertilized DBA2/B6 F1 hybrid eggs[61] by pronuclear microinjection (0.75 ng/ul per guide RNA, 10 ng/μl of repair template) and injected into pseudopregnant animals at the Mouse Genomics Core Facility (Mount Sinai).

Transgene presence was verified in founders by PCR using primers (5′–AGTCTGATGTAGGACAATGGAG–3′, 5′ –AGGATGATGACCACAAATACC– 3′) specific for the chimeric junction within the DAF-TM gene unique segment to the mouse genome. Correct site-specific integration was determined by junction PCR reactions using primer pairs (5′–AGCGGAAACGCCACTGAC–3′, 5′ –GGGCGTACTTGGCATATGAT – 3′ and 5′– AGTCTGATGTAGGACAATGGAG –3′, 5′ – GCTCCTCTGTCCACAGTTACA – 3′) that span genomic and transgenic sites at both end of the transgene.

Founder mice were backcrossed to C57BL/6J for >8 generations and then intercrossed to *Cγ1*-Cre or *CD19*-Cre animals. All experiments within the manuscript were performed with DAF-TM$^{+/+}$ mice heterozygous for either *CD19*-Cre or *Cγ1*-Cre. DAF-TM zygosity was determined using PCR primers specific for the chimeric junction part of the transgene (see primers above), and primers for the intact *Rosa26* target integration site (5′–CGACTTGAGTTGCCTCAAGAG–3′ and 5′–CCAGATGACTACCTATCCTCC–3′).

Human tissue samples

Human tonsils were obtained as de-identified, discarded surgical specimens or as de-identified archived tissue samples, with approval of the Institutional Review Board at Mount Sinai Hospital (BRC 272, IRB 11–0178) from routine tonsillectomies performed at Mount Sinai Hospital from the Biorepository and Pathology core. As such, the study is not considered human subjects research under current NIH guidelines.

Cell Lines

The human myeloma cell line KMS was purchased from the Japanese Collection of Research Bioresources Cell Bank (https://cellbank.nibiohn.go.jp/english/). The human diffuse large B cell lymphoma (DLBCL) cell lines SU-DHL-5, SU-DHL-6, SU-DHL-10, OCI-LY7, TOLEDO and the Burkitt lymphoma cell line P3HR1, were gifts of L. Pasqualucci (Columbia University Medical Center) and originally purchased from the DSMZ (www.dsmz.de) repository (SU-DHL lines and OCI-LY7) or ATCC (atcc.org) (P3HR1 and TOLEDO). Cell line identities were confirmed by multiplex cell authentication (Genetica Cell Line Testing). KMS-27 cells were cultured in RPMI 1640 Medium (Life Technologies) plus 20% heat inactivated fetal bovine serum (FBS, Life Technologies) and

1% Penicillin/Streptomycin (Life Technologies). Lymphoma cell lines were cultured in Iscove Modified Dulbecco's Medium (Life Technologies), 10% FBS (Life Technologies) 1% Pen/Strep.

Mouse immunizations

Groups of animals were immunized with SRBC (Innovative Research) or NP-KLH (BioSearch Technologies). For SRBC immunization either a single intra-peritoneal injection of 1×10^9 SRBC or sequential SRBC injections (Day 0, $1–2\times10^8$; Day 5, 1×10^9) was used as indicated. For NP-KLH,100ug of NP-KLH 1:1 vol/vol in Alum (Immject Alum, Thermofisher) was precipitated and injected intraperitoneally.

Bone marrow chimeras

Reciprocal WT CD45.1 and (CD45.2) $C3^{-/-}$ bone marrow chimeras were produced as published[62]. Eight weeks after engraftment >95% peripheral blood donor chimerism was confirmed prior to immunization.

Enzyme-Linked Immunosorbent Assay (ELISA).—Anti-SRBC titers were determined using a kit (Innovative research) to assess high affinity and total anti-NP antibodies by ELISA using BSA with different degrees of NP conjugation.[63]

DAF cleavage, Complement deposition assay

5×10^6 splenocytes from NP-KLH mice were incubated in HL-serum free media for 1h at 37°C, 5% CO_2 in the presence or absence of 5ug/ml Phospholipase C (Sigma-Aldrich), washed with PBS 1%FCS and surface DAF expression quantified by flow cytometry. Complement regulatory capacity of DAF-TM was assessed in vitro by incubating 5×10^6 splenocytes from immunized animals in 20–40% WT or *C3*$^{-/-}$ mouse serum in Annexin V buffer with 1mM $MgCl_2$ for 20min at 37°C, 5% CO_2 and quantifying C3b deposition by flow cytometry.

In vitro and in vivo GCB stimulation

In vivo stimulation.—10d after immunizing groups of control *Cγ1*-Cre$^{+/-}$, DAF-TM$^{C\gamma1}$ and Δ*C3ar1*/*C5ar1*$^{C\gamma1}$ mice with SRBC, animals were injected with anti-CD40 (150ug) and/or anti-IgM F(ab')$_2$ (100ug), or goat IgG2a (all from BioXcell) in 200ul PBS i.v. Spleens were harvested at 4h for surface staining followed by fixation, permeabilization and intracellular staining. In other studies, 20×10^6 B6 WT or C3aR1$^{-/-}$C5aR1$^{-/-}$ B cells were transferred into μMT recipients and 24 h later immunized the recipients with SRBC. On d10, animals were injected with anti-CD40 (150ug) and/or anti-IgM F(ab')$_2$ (100ug), or control goat IgG2a and the cells analyzed by flow cytometry. Serum IgM was quantified with an IgM Mouse Uncoated ELISA Kit (Invitrogen).

For in vitro studies, 10d after sequential SRBC immunization, isolated spleen cells were enriched for B cells (B cell Magnisort kit, ThermoFisher), rested for 20min at 37C, 5% CO2 in HL-media and subsequently stimulated with 10ug/ml anti-CD40, 10ug/ml anti-IgM, 0.5ug/ml murine C3a and or C5a for 20' at 37C, 5% CO2. After washing, cells were stained and analyzed cells by flow cytometry.

In vivo competition studies

Equal numbers (10^7 each) of purified CD45.2 B1–8^{hi} DAF-TM *Cγ1*-$Cre^{+/-}$ B cells (or in control experiments CD45.2 B1–8^{hi} *Cγ1*-$Cre^{+/-}$) and control CD45.1/2 B1–8^{hi} *Cγ1*-$Cre^{+/-}$ B cells were injected into CD45.1 B6 recipients. 24 h later (d0), recipient mice were immunized with 100 mg of NP-KLH, except for a set of 4 animals used as non-immunized control. Groups of animals were sacrificed at d0, 6, and 9 post-immunization and isolated splenic mononuclear cells analyzed by flow cytometry. Competitive competency indices are calculated as the percentage of each population in GCs, normalized to that in non-GC B cell fractions. This normalization minimizes the impact of varied engraftment among congenic cells in individual mice.[37]

Immunofluorescence analysis

Fixed human tonsil tissue fragments and murine draining lymph nodes and spleens (1.6% PFA 20% sucrose 4h to overnight 4°C) were incubated in PBS 15% sucrose rotating at 4°C overnight, embedded in optimum cutting temperature (OCT) compound (Tissue Tek, Sakura Finetek USA), cut in 8-micron tissue sections, fixed in cold acetone for 5 min at room temperature, then blocked in 3% bovine serum albumin (Sigma Aldrich). Sections were incubated with anti-CD35 (FITC), anti-GL7 (PE),and anti-IgD (APC) antibodies for 2 h at room temperature in blocking solution, washed with PBS, and counterstained with DAPI (VECTASHIELD, Vector Laboratories). Images were captured using a fluorescence microscope and NIS Elements v4.20 imaging software (Nikon).

Plasmids

A pMT2T backbone was used to express full-length and truncated human BCL-6 variants in transient luciferase reporter assays,. Truncated variants encode BCL-6 mutants[64] lacking either the amino-terminal transcriptional repressor domain (BCL-6-ZF) or the carboxy-terminal DNA binding zinc-finger domain (BCL-6-ΔZF), all a kind gift of K. Basso, Q. Shen and R, Dalla-Favera (Columbia University). To generate a CD55 reporter construct, PCR-amplified genomic regions spanning the human CD55 promoter (chr1:207,320,781–207,321,774; hg38 assembly) and an intronic enhancer (chr1:207,335,687–207,337,273, hg38) were subcloned into BamHI/SalI sites of pNL3.1 (Nluc minP; Promega). The promoter region, including the 5'UTR up to the ATG upstream of the NanoLuc cDNA (Nluc) was subcloned into pNL3.1 (HindIII/NcoI), replacing the ATG of Nluc with that of CD55. Promoter and enhancer regions were defined based on the span of H3K27Ac and H3K4Me1/3 marks in ChIP-Seq datasets (see Fig 2b, Extended data Fig 2).

TRE3G-BCL-6-puromycin and TRE3G-BCL-6-ZF-puromycin lentiviral vectors were constructed by subcloning a cDNA encoding full-length human BCL-6 or a truncated cDNA encoding the zinc finger DNA binding domain (ZF) downstream of a TRE3G promoter element in a modified version of pZIP-TRE3G (TransOmic). The modified vector has a UbC-rtTA-IRES-Puro cassette; all BCL-6 cDNAs were subcloned 3' of TRE3G via Gibson Assembly (NEBuilder HiFi DNA Assembly Cloning kit, New England Biolabs). BCL-6 expression is responsive to (induced by) doxycycline addition. All vector DNA and sequences are available upon request.

Electroporation and reporter assay

4×10^5 TOLEDO cells were electroporated and resuspended in buffer R (Life Technologies) using the Neon Electroporation Transfection System (Life Technologies) (10 μL tip; 1350 V; 1 pulse, 40 ms). In all transfections, 390 ng of the recombinant CD55-prom-enh-Nluc were combined with indicated amounts of pMT2T-BCL-6 or 100 ng of pMT2T-BCL-6-ZF/ pMT2T-BCL-6-ΔZF, a Firefly luciferase (FFLuc) encoding vector (pGL4.13, Promega) to control for electroporation efficiency, and pUC19 vector (NEB) for a total of 500 ng. Electroporated cells (4×10^5 cells/mL) were cultured in IMDM/10% FBS without antibiotics, and luciferase levels measured 48 h post-transfection using the Nano-Glo Dual-Luciferase Reporter Assay System (Promega). Reporter activity was reported as the ratio between Nanoluc and Firefly (transfection control) luciferase readings in multiple technical replicates across n>3 experimental replicates. Statistical significance was calculated based on the average of technical replicates in each experiment, using a Student's t-test (unpaired, two-tailed).

Lentiviral packaging and cell transduction

To generate TRE3G-puro lentiviral particles, HEK293T cells (American Type Culture Collection) were reverse transfected with TRE3G-puro lentiviral vector encoding BCL-6 or BCL-6-ZF and packaging vectors encoding REV, TAT, VSVG and GAG-Pol (10:1:1:2:1 respectively, for a total of 15μg) in a 1 mL solution of 150 mM NaCl plus 1μg/μL solution of polyethylenimine (PEI; Fisher Scientific), for a 1:4 DNA:PEI ratio. The DNA:PEI mixture was used for reverse transfection of 14×10^6 HEK293T cells in 100 mm^2 plates, incubated at 37°C. Virus-containing supernatants were harvested in two consecutive collections on day 3 and day 4, concentrated using Lenti-X concentrator (Clontech/Takara Bio), and resuspended in 1xPBS (100x suspension).

For human BCL-6 overexpression KMS-27 cells were transduced with lentiviral particles of TRE3G-BCL-6-puro at high multiplicity of infection (MOI), and selected in 1ug/mL puromycin to obtain cell pools with stable integration of the inducible transgene. Cells were cultured (1×10^6 cells in 2 mL growth medium/well) in 6-well plates and 2 μg/mL doxycycline (Dox) added to induce BCL-6 expression. Cells were harvested at 72h post-induction, stained for CD55, CD46, and CD59, fixed and permeabilized in FoxP3 staining buffer (ThermoFisher Scientific/eBioscience), stained with PE-conjugated anti-BCL-6 antibody, then analyzed by flow cytometry (FACSCalibur or Fortessa analyzers; BD).

For experiments using the dominant negative BCL-6, SU-DHL-5 cells were transduced with TRE3G-BCL-6-ZF-puro lentiviral particles at high MOI and selected with 1ug/mL puromycin for stable integration. To induce BCL-6-ZF expression, 5×10^5 cells were cultured in 2 mL growth medium ± of 2 μg/mL Dox and harvested these cells 72h post-induction. 3×10^6 cells were used to confirm overexpression of the BCL-6-ZF truncation by immunoblot, using a mouse monoclonal (H12) antibody directed against the C-terminus (ZF) domain of BCL-6.

In selected experiments, 25–50 μM BCL-6 inhibitor FX1 (Selleck Chemicals, Houston TX) dissolved in dimethyl sulfoxide was added to exponentially growing cultures of different

DLBCL and BL cell lines in fresh growth medium. Cells were harvested at 24–48h for flow cytometry analyses with anti-DAF and anti-CD46 specific antibodies (**see** Supplementary Table S3).

Immunoblot

Cells were lysed in 1% SDS lysis buffer (50 mM Tris, pH 8.0, 1 mM EDTA, 100 mM NaCl, 5 mM DTT, and 1% SDS) containing protease and phosphatase inhibitors (ThermoFisher). Lysates (10–20 ug) were resolved in Bolt® 4–12% Bis-Tris Plus gels (ThermoFisher) and MOPS buffer, transferred to nitrocellulose membranes (GE Healthcare), then incubated overnight at 4°C with primary antibodies to BCL-6 and β-actin (see Supplementary Table S3). After washing and adding horseradish peroxidase-conjugated secondary antibodies (Kindle Biosciences) assays were developed using KwikQuant Ultra Digital ECL (Kindle Biosciences). Luminescent signal was detected using a FujiFilmX-A2digital camera and raw images converted to B/W with Adobe Photoshop CS6 V13.0.

Flow Cytometry and cell sorting

Mouse spleen cell suspensions in RPMI medium were filtered (70-micron), RBCs lysed (ACK buffer, Lonza) and re-filtered (40-micron) to produce single mononuclear cell suspensions in PBS plus 1%FCS. For primary murine and human cells as well as cell lines, surface and intracellular staining were performed using antibodies listed in the Resource Table. Analyses were performed on FACS Lyric™ or Canto™ II cytometers (BD Biosciences) and the results analyzed with FlowJo software version 10.6.2 (FlowJo LLC).

GCB cells from the spleens of SRBC immunized mice were sorted after enrichment of by negative selection, using the MagniSort Mouse B cells Enrichment Kit (ThermoFisher Scientific), with addition of anti-IgD-biotin antibody to deplete IgD^+ naïve cells. GC B cell pools were sorted using $GL7^+FAS^+$ (*Cγ1*-$cre^{+/-}$ control mice) and $GL7^+FAS^+$ DAF^+ (DAF-$TM^{C\gamma1}$ mice) in a BD FACS Aria ™ III. DAF expression was used in the $GL7^+/FAS^+$ fraction to confirm transgene expression and successful recombination. In other analyses, cells in S phase were in vivo labeled for 2 h upon i.v. injection with 1 mg of 5-ethynyl-20-deoxyuridine (EdU)[65]. Cells in S phase were gated as $BrdU^+$ $7AAD^{int}$.

BCR sequencing to assess somatic hypermutation events in Vh186.2 mouse variable heavy-chain regions and Jh4 intron

Ig-lambda$^+$ GC B cells (1×10^4 flow-sorted) from DAF-$TM^{C\gamma1}$, Δ*C3ar1*/*C5ar1*$^{C\gamma1}$ and control mice 12-days post-immunization with 100μg NP-KLH, and genomic DNA isolated using the QIAamp DNA Micro Kit (Qiagen). The variable heavy-chain region 186.2–joining heavy-chain region 2 segments (Vh186.2-JH2, selected in GC responses to NP immunization[66]) were amplified by PCR using specific primer sets and 10 ng of genomic DNA and KAPA HiFi DNA Polymerase (Kapa Biosystems - Roche). The PCR protocol was previously described [5] and uses a semi-nested PCR (first PCR, outer forward primer, 5'-TCTTTACAGTTACTGAGCACACAGGAC-3' and reverse primer, 5'-GGGTCTAGAGGTGTCCCTAGTCCTTCATGACC-3'; Second PCR: inner forward primer 5'-CAGTAGCAGGCTTGAGGTCTGGAC-3' and the same reverse primer). All final PCR products were subcloned into pCR®-Blunt vector (Zero Blunt® PCR Cloning Kit, Life

Technologies) and single colonies Sanger sequenced (~40 per mouse) using a M13F-21 primer. Variable heavy-chain gene sequences were analyzed using HighV-Quest (The International Immunogenetics Information System, IMGT)[67, 68], identifying unique sequences (clones) matching the V186.2 gene (IGHV1–72*01). Differences in the frequency of clones with high affinity mutations between groups were determined using Fisher's Exact test. A Chi-square test was used to compare the total mutations within VH segments and mutation frequency per 100bp in different groups. Statistical differences in the total number of mutations per segment were calculated using a Mann-Whitney test.

For the sequencing and analysis of hypermutation events at Jh4 intronic regions, a 591 bp region from genomic DNA was amplified for 35 cycles using a high-fidelity polymerase (KAPA HiFi, KAPA Biosystems-Roche) and gene-specific primers[69]: *JH4int-F:* TCCTAGGAACCAACTTAAGAGT; *JH4int-R:* TGGAGTTTTCTGAGCATTGCAG. The products were cloned in the pCR-Blunt II vector (Zero Blunt PCR cloning kit, Thermofisher) and sequenced using M13 primers via Sanger sequencing (~20–25 clones per mouse, 3 mice per genotype). All identical sequences were removed using *ElimDupes* (https://www.hiv.lanl.gov/content/sequence/elimdupesv2/elimdupes.html) and unique sequences aligned to a consensus reference sequence using *SHMTool*[69]. The sequence in *Cγ1*-Cre mice differs from the C57BL/6 germline sequence at 5 nucleotide positions. Statistical significance in mutation frequencies was determined using the Mann-Whitney test (Graphpad Prism, v 8.4.2). See Supplementary Table 1 for a detailed summary of the BCR sequencing results.

RNA isolation and quality control

Total RNA was isolated from sorted, viable germinal center B cells ($B220^+GL7^+Fas^+$) from *Cγ1*$cre^{+/-}$ control and DAF-$TM^{Cγ1}$ mice using the Direct-zol™ RNA MicroPrep kit (Zymo Research, Irvine CA). The purified RNA was eluted in DNase/RNase-Free Water and quantified by NanoDrop spectrophotometer and quality assessed (RNA integrity number) in an Agilent 2100 Bioanalyzer using a RNA 600 pico kit.

RNA-seq

10 ng of total RNA was processed with RIN scores > 5 to generate libraries for RNA-seq using the SMART-seq v4 Ultra Low Input RNA kit (Takara). Libraries were multiplexed and sequenced on an Ilumina NextSeq 550 instrument, to a minimum of 30 million single-end 100 base pair reads. HISAT2 v2.1.0 [70] was used to align Fastq reads to the Mus musculus genome (mm10) using with options –dta –trim5 5 –add-chrname –ignore-quals -q -k 1; and *featureCounts* [71] with options -T −4 -exon -g gene_name to generate raw counts from aligned BAM files. Raw read counts were used as input for the differential expression analysis using DESeq2 v 1.10.1 [72]. The table output of DESeq2 (82 genes, p.adj value <0.05; see Supplementary Table 2) was used for pathway enrichment analyses using the Broad Institute Molecular Signatures Database (MSigDB, *Interrogate gene sets* tool, hypergeometric distribution p-values); or the Gene Set Enrichment Analysis tool (GSEA v4.0.3)[39] with selected signatures (Fig 5–6, Extended data Fig 7) with the following settings: 'Permutations' -gene set; 'Enrichment Statistic' -weighted and 'Metric for Ranking Genes' -Signal2Noise. For unbiased hierarchical clustering of gene expression data, raw counts were

converted to TPM, then used as input in the *HierarchicalClustering* module in GenePattern[73] (Pearson correlation, average linkage). A detailed summary of these analyses can be found in Supplementary Table 2.

Analysis of public gene expression data and heat map rendering

The gene expression heatmaps and gene expression graphs (Fig. 1e) show publicly available data from the Immunological Genome Project (ImmGen; mouse) and the Gene Expression Omnibus (GEO) (https://www.ncbi.nlm.nih.gov/geo/), records GSE2350 (human tonsil B cell subsets) and GSE139833. To generate the heatmaps, gene expression values were standardized (z-scores) across samples (rows) and then used the scaled data for heatmap generation using the *HeatMap Viewer* tool in the GenePattern server (genepattern.org).

Quantification and Statistical Analysis

GraphPad Prism Software (version 8.4.2) was used for all statistical analyses. Details for each statistical test are indicated in the corresponding figure legends and in the methods sections. Significance levels (p-value) are also reported in each figure legend. For RNA-Seq experiments, 4 independent mice donors per genotype were used and correct sample clustering confirmed using Principal Component Analysis prior to differential expression analysis.

For in vivo experiments, sample size was determined using G*Power[74] (80% Power, significance level -alpha <0.05 and standard deviation determined from previous studies on GC development), to detect differences >20% between groups in cell percentages, cell numbers or marker expression levels using two-tailed tests.

Extended Data

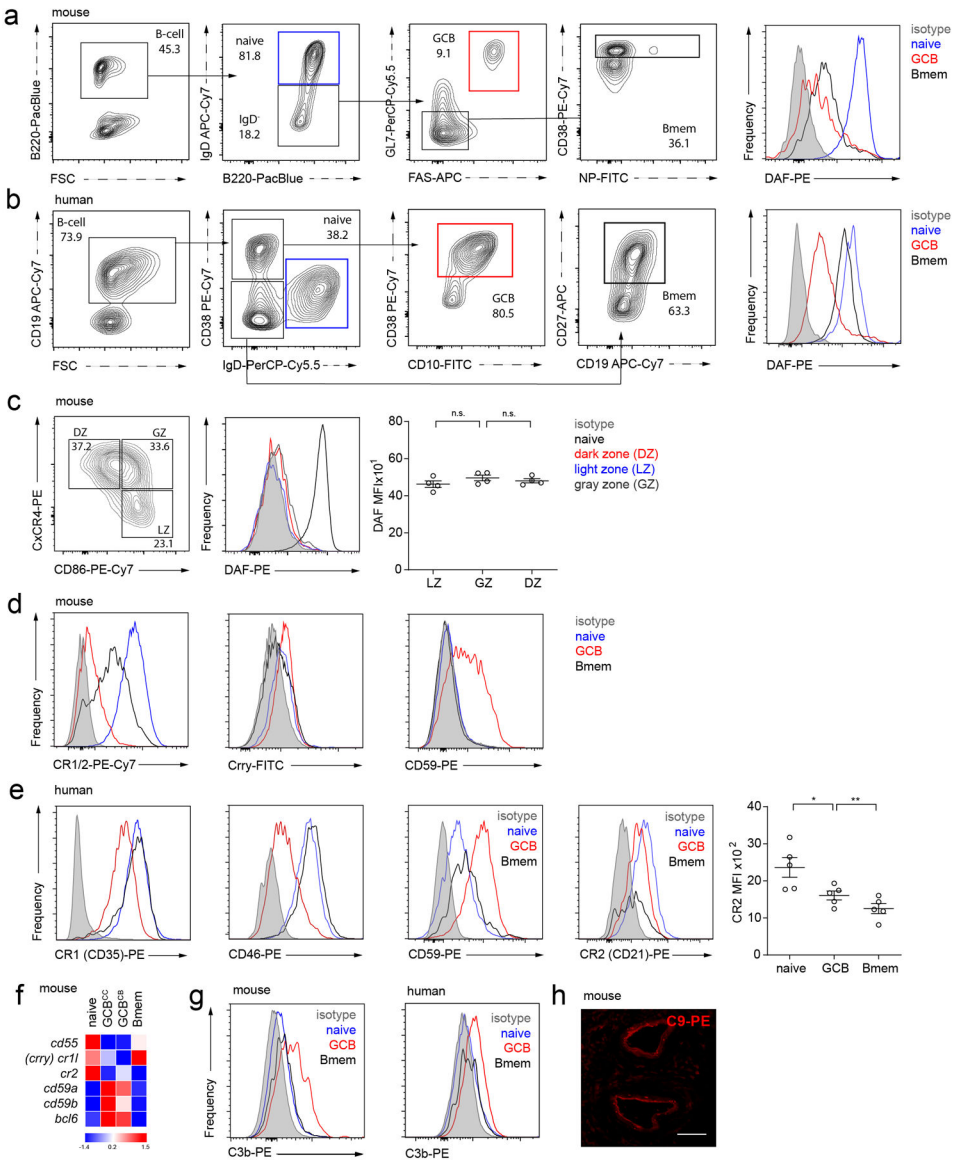

Extended Data Fig. 1. Distribution of complement regulator expression in mature B cell subsets

a-b. Gating strategy for flow cytometry analysis of murine (**a**) and human (**b**) naïve, GC and memory B cells, with representative histograms of DAF expression across B cell subsets. **c**. DAF expression on light (LZ), dark (DZ) and grey zone (GZ) GC B cells defined by CXCR4 and CD86 expression (left) with representative histograms (middle) and quantitation (right). **d.** Representative flow plots of mouse B cell subsets for CR1/2, Crry, and CD59 expression. **e.** Representative histograms of human tonsillar B cell subsets for CR1(CD35), CD46, CD59 and CR2(CD21) expression, with quantitation of CR2/CD21 expression (right panel) **f.** Heat map, source: ImmGen database, with row-normalized mRNA expression of complement regulators and *Bcl6* in different murine B cell subsets. **g**. Representative histograms showing C3b staining on murine (left) and human (right) B cell subsets. **h.** Representative (3 individual experiments) image of human tonsil staining with anti-C9 showing positive

staining of vascular endothelium (positive control for Fig 1g), scale bar 50 μm. Data are presented as MFI +/− SEM, *p<0.05, **p<0.01, ***p<0.005 by ANOVA with Bonferroni post-test (**c,e**). Each dot represents a biological replicate. n.s., not significant

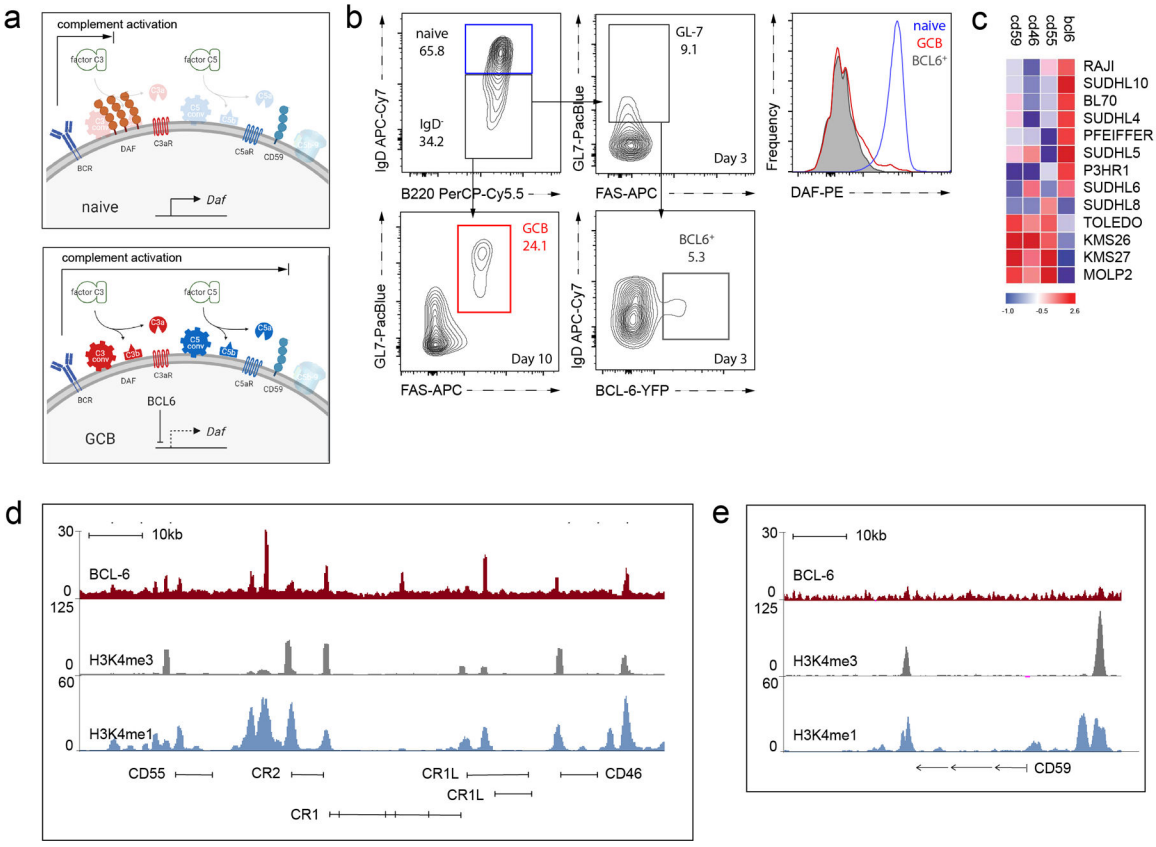

Extended Data Fig. 2. BCL6 is inversely correlated with DAF expression and binds to regulatory regions of RCA genes.

a. Schematic diagram illustrating effects of absent DAF with persistent CD59 expression on complement activation products on naïve (top) vs GC (bottom) B cells. **b.** Gating strategy for DAF/CD55 expression on immunized BCL6-YFP^{+} reporter mice, d3 post-immunization with SRBCs including d10 naïve and GC B cell controls (complementary to Fig 2a). **c**. Heat map depicting relative mRNA expression levels (row-normalized) for BCL6 and complement regulators on human B cell lymphoma cell lines (Diffuse Large B cell lymphoma and selected Burkitt lymphoma cell lines: Raji, BL70, P3HR1; and Multiple Myeloma cell lines: KMS26, KMS27 and MOLP2). Data extracted from the Cancer Cell Line Encyclopedia (CCLE) repository [1, 2]. (**d-e**) Schematic depiction of ChIP-seq tracks for BCL6 and selected histone marks at the human RCA (**d**) and CD59 (**e**) gene loci. Data extracted from GEO records GSE68349, GSE67494 [3, 4].

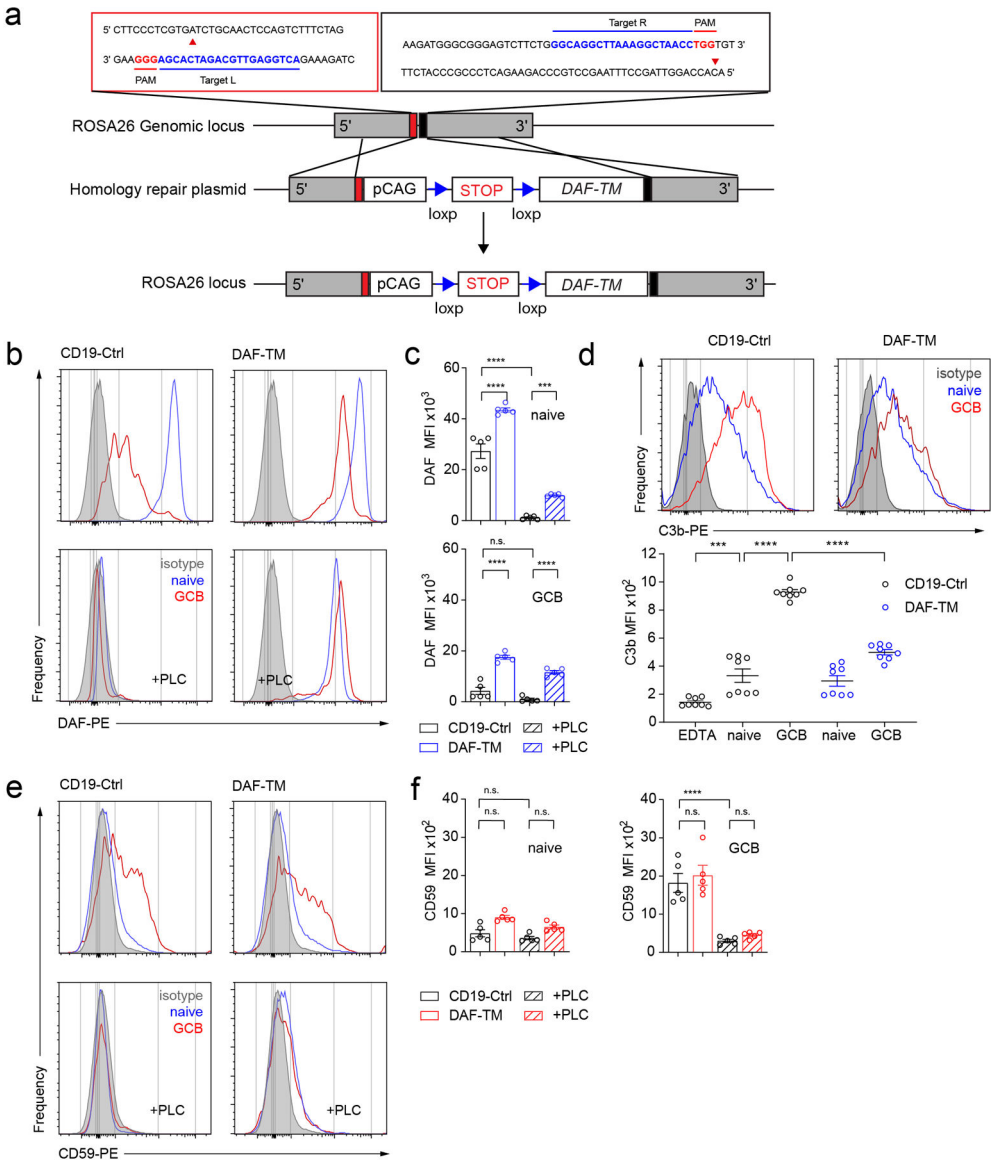

Extended Data Fig. 3. Design and validation of conditional DAF-TM transgenic mice.

a. Schematic of Crispr/Cas9n strategy for producing DAF-TM transgenic mouse. The sequence inset shows a segment of the WT *Rosa26* locus and our targeting gRNA design. The PAM (Protospacer Adjacent Motif) is highlighted in red. The 5'–NGG–3' sequence is the PAM consensus for binding of S. pyogenes Cas9 and Cas9D10A (Cas9n) nickase variant. The sequences in blue adjacent to the PAM sequences (Target L and Target R) indicate the target sites for Cas9n mediated cleavage. These sequences are identical with the spacer sequences in gRNA-A and gRNA-B, respectively. Cas9n nicks the target DNA at sites indicated with red triangles. Offset nicking induces recombination between the genomic *Rosa26* locus and the homology arms in the repair plasmid that results in insertion of the DAF-TM transgenic construct between the WT *Rosa26* segments indicated with red and black boxes. **b-c.** Representative flow cytometry plots (**b**) and quantified results (**c**) of DAF staining on naïve and GC B cells from DAF-TM^{CD19} mice (DAF-TM x *CD19*-Cre$^{+/-}$)

and CD19$^{+/-}$ control mice in the absence or presence of phospholipase C (PLC), n=5 independent biological replicates. Note that PLC totally removes native surface DAF from Control (*CD19*-Cre$^{+/-}$) B cells. In DAF-TM^{CD19} B cells, PLC removed native (GPI-anchored) DAF leaving lower but detectable levels of transgenic DAF resistant to PLC cleavage. **d**. Representative histograms (top) and quantification (bottom) depicting lower C3b deposition on B cell subsets from DAF-TM^{CD19} compared to control *CD19*-Cre$^{+/-}$ mice. **e-f**. Representative flow cytometry plots (**e**) and quantified results (**f**) of CD59 staining on naïve and GC B cells from DAF-TM^{CD19} (DAF-TM x *CD19*-Cre$^{+/-}$) and *CD19*-Cre$^{+/-}$ control mice in the absence or presence of phospholipase C (PLC), n=5 independent biological replicates. PLC removed the GPI-anchored CD59 from the surfaces of GC B cells in both *CD19*-Cre$^{+/-}$ and DAF-TM^{CD19} B cells.; All data are presented as MFI +/− SEM, *p<0.05,**p<0.01, ***p<0.005, ****p<0.001 by one-way ANOVA with Bonferroni post-test (**c,d,f**). n.s., not significant. Each dot represents a biological replicate.

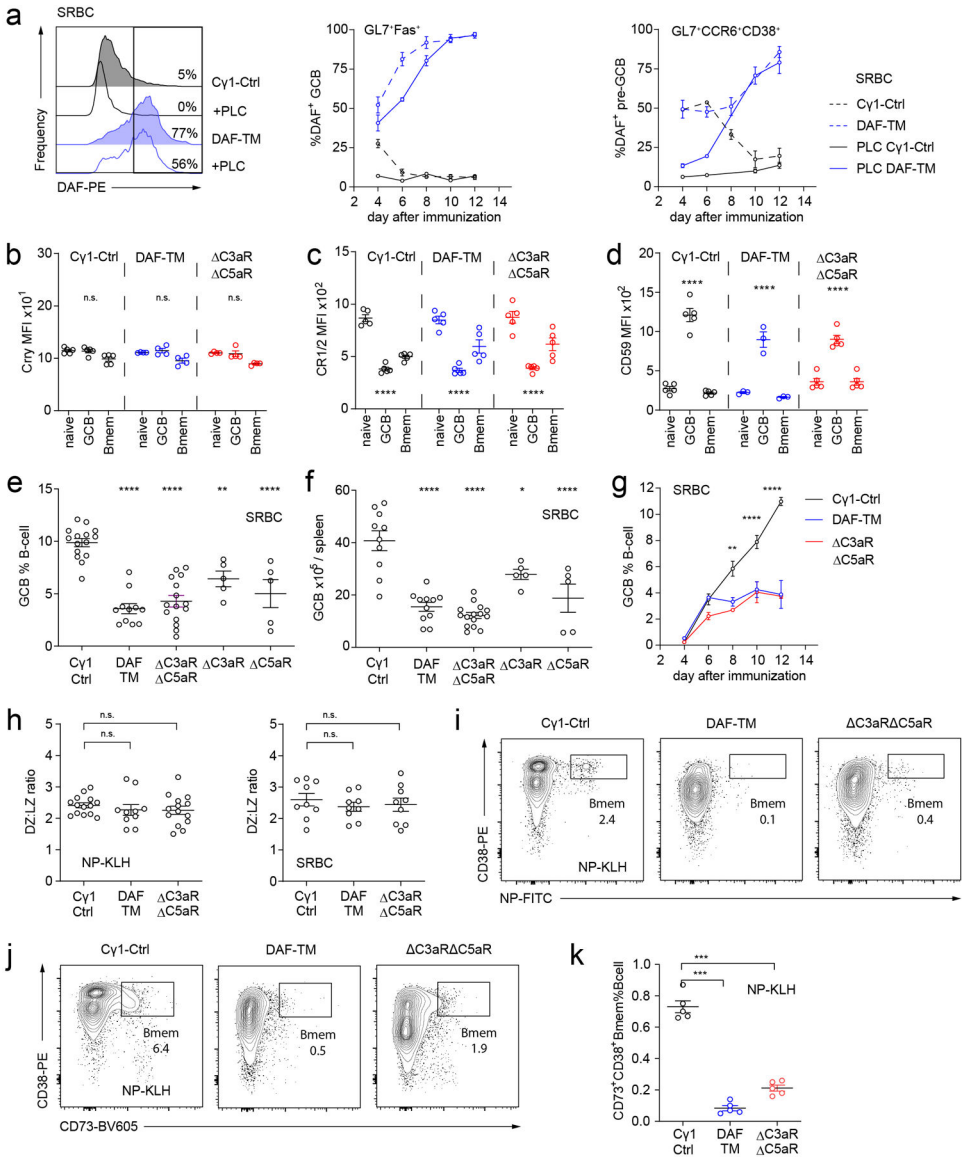

Extended Data Fig. 4. Extended characterization of GC and antibody responses in GC- (*Cγ1*-Cre) and B cell-specific (CD19-cre) DAF-TM and ΔC3aR1, ΔC5aR1 mice

a. representative histograms (left) and kinetics of total surface DAF and DAF-TM (PLC-resistant) expression on IgD^{-}Fas^{+}GL7^{+} GC B cells (middle) and IgD^{-}GL7^{+}CCR6^{+}CD38^{+} B cells (right) in DAF-TM$^{C\gamma1}$ (DAF TM) and control *Cγ1*-Cre$^{+/-}$ (Cγ1 Ctrl) mice. Note the progressive accumulation of DAF-TM^{+} B cells over time, following the kinetics of *Cγ1*-Cre-driven recombination.[5] **b-d.** Quantified surface expression of Crry (**b**) CR1/2 (**c**), and CD59 (**d**) proteins on B cell subsets from *Cγ1*-Cre$^{+/-}$ control, DAF-TM$^{C\gamma1}$ and, Δ*C3ar1*/*C5ar1*$^{C\gamma1}$ mice. **e-f.** Relative % (**e**) and absolute frequencies (**f**) of splenic GC B cells in d12 SRBC-immunized DAF-TM$^{C\gamma1}$ (DAF TM), Δ*C3ar1*/*C5ar1*$^{C\gamma1}$ (ΔC3aRΔC5aR) *C3ar1*$^{C\gamma1}$ (ΔC3aR), Δ*C5ar1*$^{C\gamma1}$ (ΔC5aR), and control *Cγ1*-Cre$^{+/-}$ (Cγ1 Ctrl) mice. **g.** Kinetics of relative GC B cells frequencies in SRBC immunized DAF-TM$^{C\gamma1}$, Δ*C3ar1*/*C5ar1*$^{C\gamma1}$ and *Cγ1*-Cre$^{+/-}$ mice. **h**. Ratios of DZ (CXCR4^{+}CD86^{+}) vs LZ (CXCR4^{-}CD86^{+}) GC B cells d10 post-immunization with NP-KLH (left) or SRBC (right). **i.** Representative flow

cytometry plots for $CD38^{+}NP^{+}$ memory B cells (Bmem), within $B220^{+}IgD^{-}GL7^{-}Fas^{-}$ spleen cell populations of NP-KLH-immunized *Cγ1*-$Cre^{+/-}$ control, DAF-$TM^{C\gamma1}$ and Δ*C3ar1*/*C5ar1*$^{C\gamma1}$ mice (d12 post-immunization) (see also Figure 3f). **j-k**. Representative flow cytometry plots **(j)** and quantified results **(k)** for $CD38^{+}CD73^{+}$ Bmem gated on $B220^{+}IgD^{-}GL7^{-}Fas^{-}$ spleen cells in NP-KLH-immunized *Cγ1*-$Cre^{+/-}$ control, DAF-$TM^{C\gamma1}$ and Δ*C3ar1*/*C5ar1*$^{C\gamma1}$ mice on d12. Data are presented as MFI (**b-d**) or mean (**a**, **e-h**, **k**) +/− SEM *p<0.05, **p<0.01, ***p<0.005, ****p<0.001 by ANOVA with Bonferroni post-test (**a-h**, **k**), For kinetics in (**g**), 3 genotypes were compared at each time point. Each dot represents a biological replicate. n.s., not significant

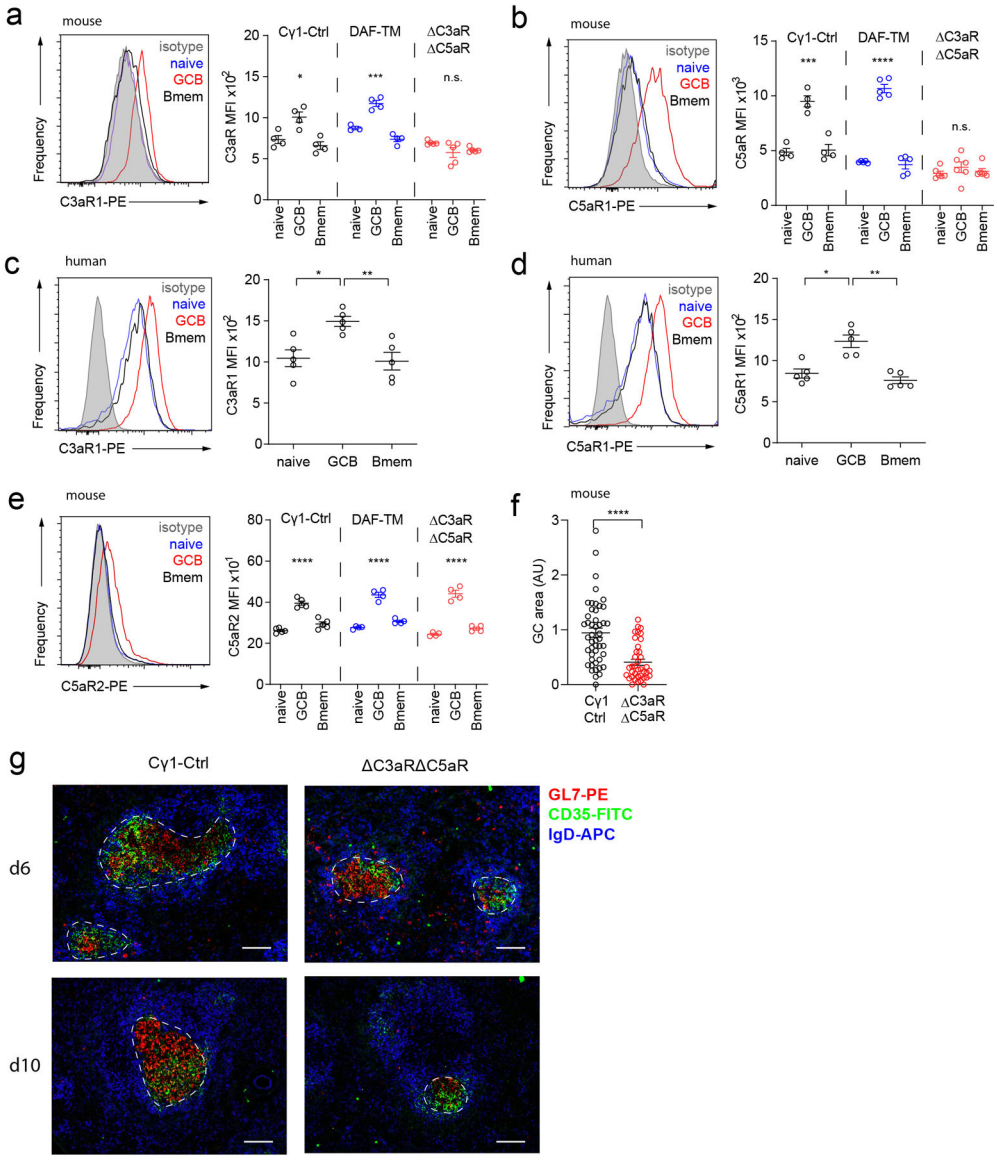

Extended Data Fig. 5. Analysis of C3aR1 and C5aR1 Expression in mouse and human B cell subsets

a-b. Representative histograms (left panels) and quantified results (right panels) for C3aR1 **(a)** or C5aR1 **(b)** expression on splenic B cell subsets of immunized control *Cγ1*-$Cre^{+/-}$

mice. **c-d.** Representative histograms (left panels) and quantified results (right panels) for C3aR1 (**c**) and C5aR1 (**d**) expression on human tonsil B cell subsets. **e.** Representative histograms (left panels, *Cγ1*-Cre$^{+/-}$ mice) and quantified results (right panel) for C5aR2 (C5L2) expression on B cell subsets from DAF-TM$^{C\gamma1}$ (DAF TM), Δ*C3ar1*/*C5ar1*$^{C\gamma1}$ (ΔC3aRΔC5aR), and control *Cγ1*-Cre$^{+/-}$ (Cγ1 Ctrl) mice on d10 after NP-KLH immunization. (**f**) Quantified GC sizes on d10 post-immunization and (**g**) representative IF images of GCs from d6 and d10 Δ*C3ar1*/*C5ar1*$^{C\gamma1}$ and *Cγ1*-Cre$^{+/-}$ mice post-SRBC immunization (spleen). Dotted lines in (**g**) outline GCs. Scale bar 50μm. Data derived from 3 different tissue sections from each of 3 individual animals. Data are presented as MFI (**a-e**) or mean (**f**) ± SEM, *p<0.05, **p<0.01, ***p<0.005 by ANOVA with Bonferroni post-test (**a-e**) or Students t-test (**f**). n.s., not significant. Each dot represents a biological replicate.

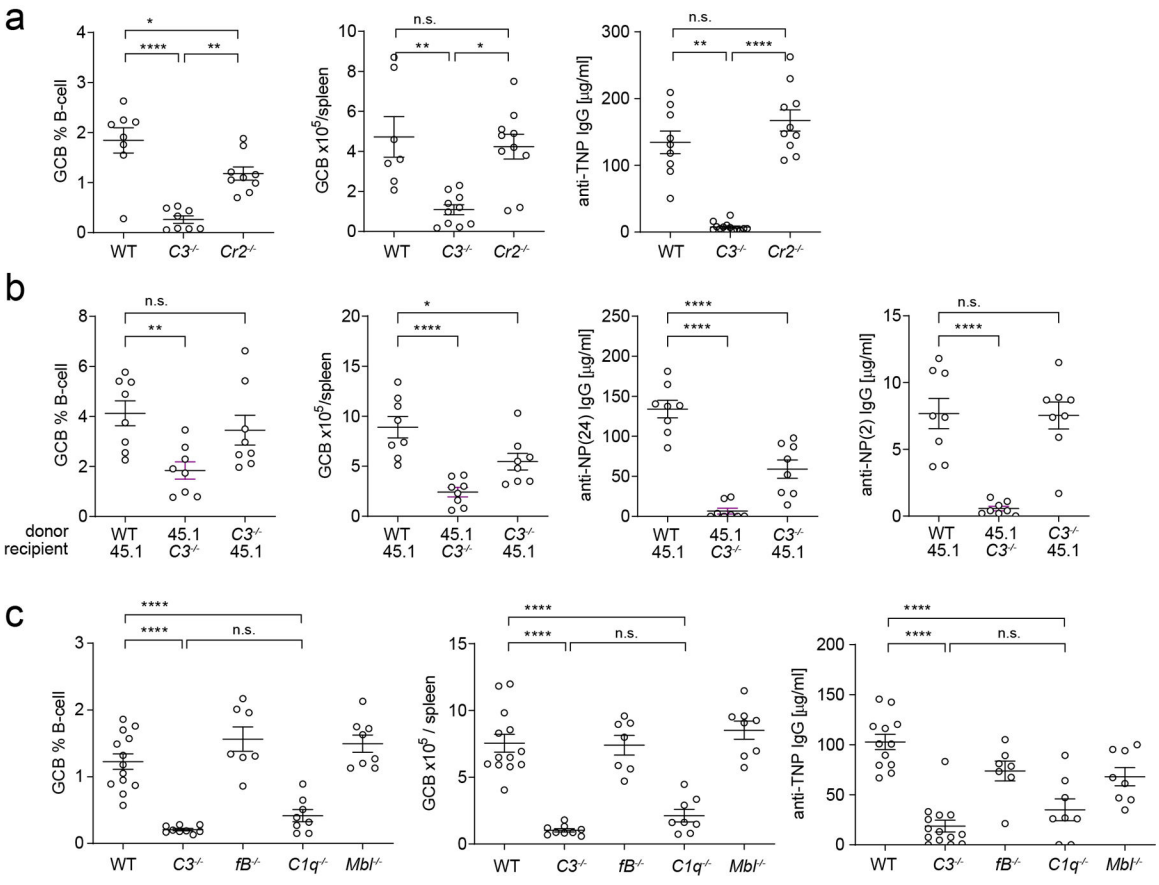

Extended Data Fig. 6. Characterization of mouse GC and antibody responses in absence of CD21 or complement component expression

a. Relative (left), absolute frequency (middle) of GC B cells and serum anti-TNP antibodies (right panel) in groups of WT and germline, congenic, cohoused *C3*$^{-/-}$ and *Cr1*$^{-/-}$ (*Cr2*$^{-/-}$, CD21 null) mice on d14 after immunization with TNP-KLH (CR1 and CR2/CD21 derive from alternatively spliced transcripts from a single gene in mice). **b.** Quantified GC B cells (left 2 panels) and serum anti-NP antibodies (total, 3rd panel, high affinity 4th panel) in C3 BM chimeras and controls (see Methods). **c.** Relative (left), absolute frequency (middle) of GC B cells and serum anti-TNP antibodies (right panel) in groups of WT and germline

congenic cohoused *C3*$^{-/-}$, *fB*$^{-/-}$, *C1q*$^{-/-}$ and *Mbl1*$^{-/-}$*Mbl2*$^{-/-}$ (*Mbl*$^{-/-}$) mice on d14 after immunization with TNP-KLH. Data are presented as mean ± SEM; *p<0.05, **p<0.01, ***p<0.005, ****p<0.001, by ANOVA with Bonferroni post-test. n.s. not significant. Each dot represents a biological replicate.

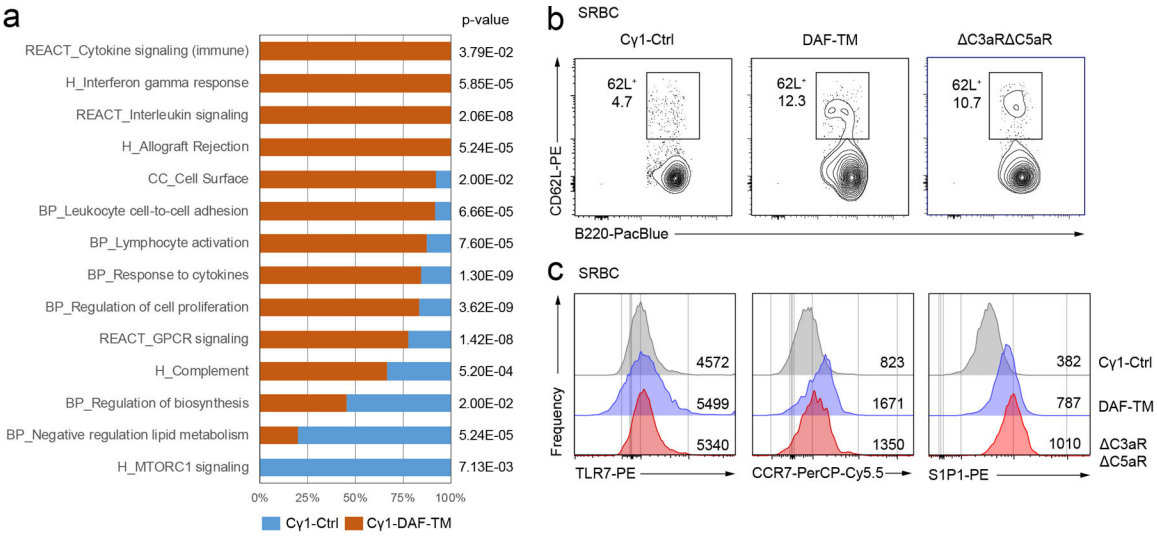

Extended Data Fig. 7. Extended data for RNA-seq and surface marker signatures of GC B cells in DAF-TM^{Cγ1}, Δ*C3ar1*/*C5ar1*^{Cγ1} and *Cγ1*-Cre$^{+/-}$ mice

a. General summary of curated pathways up- or downregulated in RNA-seq gene expression datasets (relative enrichment) from DAF-TM^{Cγ1} (DAF TM) and control *Cγ1*-Cre$^{+/-}$ (*Cγ1* Ctrl) mice (see also Extended Data Table 2). p-values hypergeometric distribution based on gene overlaps, with FDR q-value <0.05 (p-value after Benjamini and Hochberg correction for multiple hypothesis testing). **b.** Representative flow cytometry plots depicting the percentage of CD62L^{+} GC B cells from DAF-TM^{Cγ1} (DAF TM), Δ*C3ar1*/*C5ar1*^{Cγ1} (ΔC3aRΔC5aR), and control *Cγ1*-Cre$^{+/-}$ (Cγ1 Ctrl) mice on d10 after immunization with SRBC. **C.** Representative flow cytometry histograms for TLR7, CCR7 and S1P1 gated on IgD^{-}GL7^{+}Fas^{+} GC B cells from DAF-TM^{Cγ1}, Δ*C3ar1*/*C5ar1*^{Cγ1} and *Cγ1*-Cre$^{+/-}$ mice on d10 after immunization with SRBC (numbers correspond to MFI values).

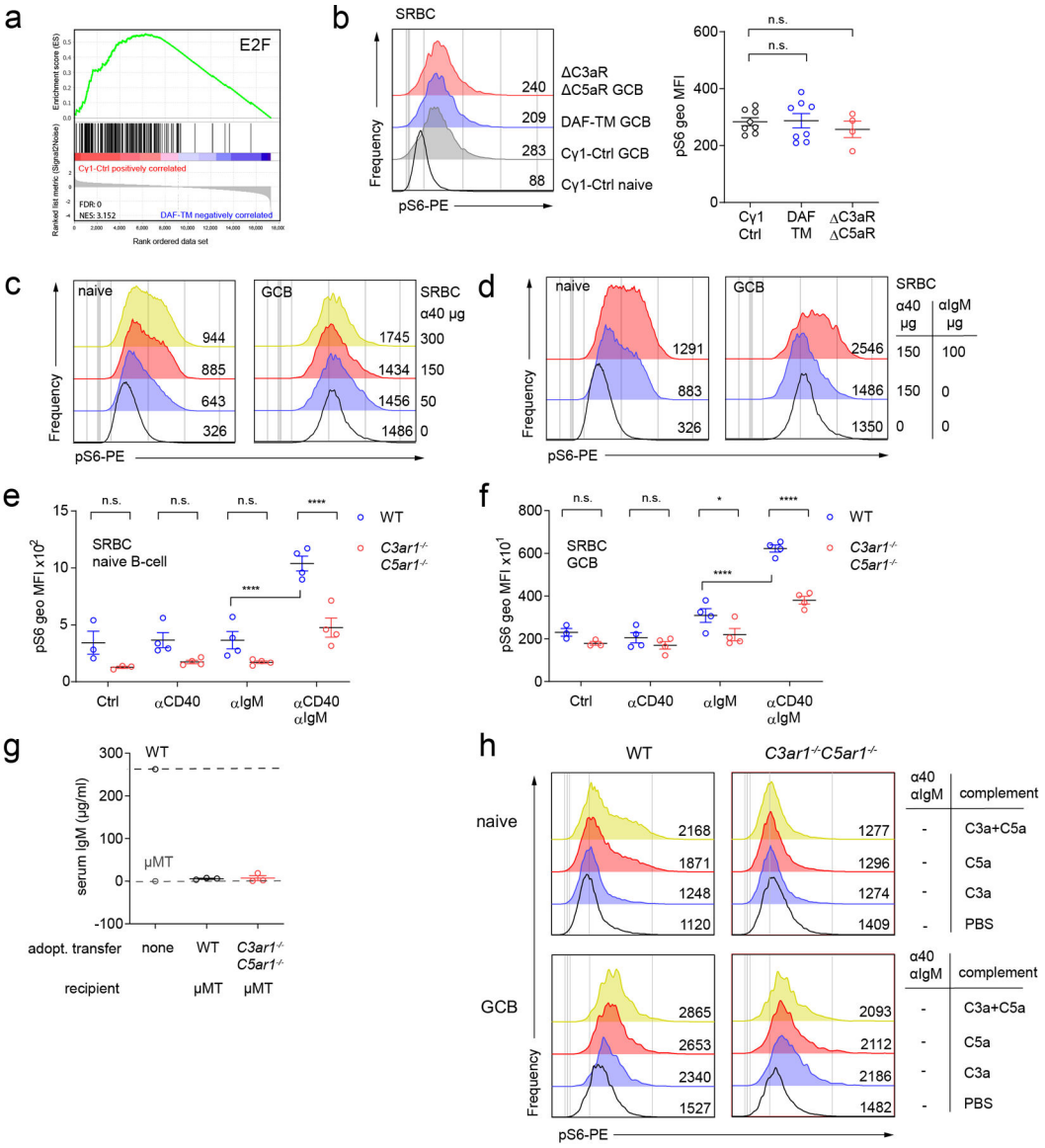

Extended Data Fig. 8. Extended data and experimental controls for RNA-seq analysis and mTOR signaling responses to CD40 and C3aR1/C5aR1 ligation

a. GSEA enrichment plot for E2F gene signature in DAF-TM^{Cg1} vs. *Cγ1*-Cre$^{+/-}$ mice. NES, normalized enrichment score; FDR, false discovery rate (see also Extended Data Table 2). **b.** Representative histograms (left) and MFI (right) of pS6 levels in GC B cells (filled histograms) from DAF-TM^{Cγ1} (DAF TM), Δ*C3ar1*/*C5ar1*^{Cγ1} (ΔC3aRΔC5aR), and control *Cγ1*-Cre$^{+/-}$ (Cγ1 Ctrl) at d10 post-SRBC immunization (without anti-CD40 or anti-IgM F(ab')$_2$ stimulation). **c-d**. Representative histograms for pS6 levels in naïve (left) or GC B cells (right) from DAF-TM^{Cγ1}, Δ*C3ar1*/*C5ar1*^{Cγ1} and *Cγ1*-Cre$^{+/-}$ mice on d10 after SRBC immunization and 4h after i.v. anti-CD40 antibody at the indicated dose (**c**), or anti-CD40+anti-IgM F(ab')$_2$ as indicated. **e-g.** 2×10^7 WT or C3aR1$^{-/-}$C5aR$^{-/-}$ B cells were transferred into μMT recipients, which were subsequently immunized with SRBC. Levels of pS6 were quantified in GC (**e**) or naïve B cells (**f**) d10 post-immunization and 4 h after i.v anti-CD40/anti-IgM F(ab')$_2$ stimulation. **g**. ELISA for serum IgM in adoptive hosts (d10),

including μMT negative and a WT B6 positive controls. **h**. Representative pS6 staining histograms of *in vitro* cultured naïve (top) and GC (bottom) B cells, stimulated for 20 min ± recombinant C3a, C5a (alone), without anti-CD40/ anti-IgM F(ab')$_2$ stimulation. n=5/group, 2 independent experiments. Data are presented as MFI (**b**, **e-f**) or mean (**g**) +/− SEM, *p<0.05, **p<0.01, ***p<0.005, ****p<0.001, by ANOVA with Bonferroni post-test (**b, e-f**). n.s, not significant. Each dot represents a biological replicate.

Supplementary Material

Refer to Web version on PubMed Central for supplementary material.

Acknowledgements

The authors thank the Mount Sinai Biorepository and Pathology Core, The Mount Sinai Mouse Genetics Core (K. Kelley, director), The Mount Sinai Flow cytometry core, and The Mount Sinai Microscopy Core, and the Genomics Core for their technical assistance. The authors thank Y. Garcia-Carmona, L. Anderson, Denise Peace, and N. Samuel-Stokes (Icahn School of Medicine at Mount Sinai) for technical assistance, and C. Cunningham-Rundles (Icahn School of Medicine at Mount Sinai), R. Fairchild (Cleveland Clinic, Cleveland OH) and F. Lin (Cleveland Clinic, Cleveland OH) for critical comments/advice.

Funding:

This research was funded through NIH R01-AI141434 (awarded to PSH and DDS), NIH R21 AI 071185 (to PSH and DH and SAL), and NIH/NCI Cancer Center Support grant P30-CA196521 to the Tisch Cancer Institute at Mount Sinai. AC was supported by a fellowship grant from the American Society of Transplantation, GV by a postdoctoral fellowship of the Lymphoma Research Foundation, and MPR by a Ruth L. Kirchstein National Service Award (NRSA) Institutional Research Training Grant (T32-C078207). FO was supported by an Institutional Research Training Grant (T32-CA078207).

Data Availability Statement.

RNA-Seq datasets were deposited in the Gene Expression Omnibus (GEO) database under accession number GSE148570 (reference series). Additional pre-processed data is provided in Supplementary Tables 1 and 2. Data from publicly available datasets were used for additional analyses, as specified in the figure legends: Gene Expression Omnibus (https://www.ncbi.nlm.nih.gov/geo/) datasets, records GSE2350, GSE139833 (human tonsil B cell subsets); GSE68349 and GSE67494 (chromatin immunoprecipitation data for BCL-6 and histone marks in human GC B cells). Immunological Genome Project (ImmGen; https://www.immgen.org) for mouse B cell subset gene expression data.

References

1. Victora GD & Nussenzweig MC Germinal centers. Annu Rev Immunol 30, 429–457 (2012). [PubMed: 22224772]
2. Shlomchik MJ, Luo W & Weisel F Linking signaling and selection in the germinal center. Immunological reviews 288, 49–63 (2019). [PubMed: 30874353]
3. Ersching J et al. Germinal Center Selection and Affinity Maturation Require Dynamic Regulation of mTORC1 Kinase. Immunity 46, 1045–1058 e1046 (2017). [PubMed: 28636954]
4. Luo W, Weisel F & Shlomchik MJ B Cell Receptor and CD40 Signaling Are Rewired for Synergistic Induction of the c-Myc Transcription Factor in Germinal Center B Cells. Immunity 48, 313–326 e315 (2018). [PubMed: 29396161]
5. Schwickert TA et al. A dynamic T cell-limited checkpoint regulates affinity-dependent B cell entry into the germinal center. J Exp Med 208, 1243–1252 (2011). [PubMed: 21576382]

6. Srinivasan L et al. PI3 kinase signals BCR-dependent mature B cell survival. Cell 139, 573–586 (2009). [PubMed: 19879843]
7. Dominguez-Sola D et al. The proto-oncogene MYC is required for selection in the germinal center and cyclic reentry. Nat Immunol 13, 1083–1091 (2012). [PubMed: 23001145]
8. Heeger PS et al. Decay-accelerating factor modulates induction of T cell immunity. J Exp Med 201, 1523–1530 (2005). [PubMed: 15883171]
9. Lalli PN et al. Locally produced C5a binds to T cell-expressed C5aR to enhance effector T-cell expansion by limiting antigen-induced apoptosis. Blood 112, 1759–1766 (2008). [PubMed: 18567839]
10. Strainic MG et al. Locally produced complement fragments C5a and C3a provide both costimulatory and survival signals to naive CD4+ T cells. Immunity 28, 425–435 (2008). [PubMed: 18328742]
11. Verghese DA et al. C5aR1 regulates T follicular helper differentiation and chronic graft-versus-host disease bronchiolitis obliterans. JCI Insight 3, 10.1172/jci.insight.124646 (2018).
12. Medof ME, Kinoshita T & Nussenzweig V Inhibition of complement activation on the surface of cells after incorporation of decay-accelerating factor (DAF) into their membranes. J Exp Med 160, 1558–1578 (1984). [PubMed: 6238120]
13. Carroll MC et al. Organization of the genes encoding complement receptors type 1 and 2, decay-accelerating factor, and C4-binding protein in the RCA locus on human chromosome 1. J Exp Med 167, 1271–1280 (1988). [PubMed: 2451706]
14. Jacobson AC & Weis JH Comparative functional evolution of human and mouse CR1 and CR2. J Immunol 181, 2953–2959 (2008). [PubMed: 18713965]
15. Kennedy DE et al. Novel specialized cell state and spatial compartments within the germinal center. Nat Immunol 21, 660–670 (2020). [PubMed: 32341509]
16. Basso K & Dalla-Favera R Roles of BCL6 in normal and transformed germinal center B cells. Immunological reviews 247, 172–183 (2012). [PubMed: 22500840]
17. Kitano M et al. Bcl6 protein expression shapes pre-germinal center B cell dynamics and follicular helper T cell heterogeneity. Immunity 34, 961–972 (2011). [PubMed: 21636294]
18. Dominguez-Sola D et al. The FOXO1 Transcription Factor Instructs the Germinal Center Dark Zone Program. Immunity 43, 1064–1074 (2015). [PubMed: 26620759]
19. Basso K et al. Integrated biochemical and computational approach identifies BCL6 direct target genes controlling multiple pathways in normal germinal center B cells. Blood 115, 975–984 (2010). [PubMed: 19965633]
20. Cardenas MG et al. Rationally designed BCL6 inhibitors target activated B cell diffuse large B cell lymphoma. J Clin Invest 126, 3351–3362 (2016). [PubMed: 27482887]
21. Rickert RC, Roes J & Rajewsky K B lymphocyte-specific, Cre-mediated mutagenesis in mice. Nucleic Acids Res 25, 1317–1318 (1997). [PubMed: 9092650]
22. Casola S et al. Tracking germinal center B cells expressing germ-line immunoglobulin gamma1 transcripts by conditional gene targeting. Proc Natl Acad Sci U S A 103, 7396–7401 (2006). [PubMed: 16651521]
23. Lalli PN, Strainic MG, Lin F, Medof ME & Heeger PS Decay accelerating factor can control T cell differentiation into IFN-gamma-producing effector cells via regulating local C5a-induced IL-12 production. J Immunol 179, 5793–5802 (2007). [PubMed: 17947652]
24. Verghese DA et al. T Cell Expression of C5a Receptor 2 Augments Murine Regulatory T Cell (TREG) Generation and TREG-Dependent Cardiac Allograft Survival. J Immunol 200, 2186–2198 (2018). [PubMed: 29436411]
25. Mayer CT et al. The microanatomic segregation of selection by apoptosis in the germinal center. Science 358, science.aao2602 (2017).
26. Hebell T, Ahearn JM & Fearon DT Suppression of the immune response by a soluble complement receptor of B lymphocytes. Science 254, 102–105 (1991). [PubMed: 1718035]
27. Wentink MW et al. CD21 and CD19 deficiency: Two defects in the same complex leading to different disease modalities. Clin Immunol 161, 120–127 (2015). [PubMed: 26325596]

28. Jolly CJ, Klix N & Neuberger MS Rapid methods for the analysis of immunoglobulin gene hypermutation: application to transgenic and gene targeted mice. Nucleic Acids Res 25, 1913–1919 (1997). [PubMed: 9115357]
29. Inoue T et al. The transcription factor Foxo1 controls germinal center B cell proliferation in response to T cell help. J Exp Med 214, 1181–1198 (2017). [PubMed: 28351982]
30. Pereira JP, Kelly LM, Xu Y & Cyster JG EBI2 mediates B cell segregation between the outer and centre follicle. Nature 460, 1122–1126 (2009). [PubMed: 19597478]
31. Klein U et al. Transcriptional analysis of the B cell germinal center reaction. Proc Natl Acad Sci U S A 100, 2639–2644 (2003). [PubMed: 12604779]
32. Gatto D, Wood K & Brink R EBI2 operates independently of but in cooperation with CXCR5 and CCR7 to direct B cell migration and organization in follicles and the germinal center. J Immunol 187, 4621–4628 (2011). [PubMed: 21948984]
33. Cyster JG et al. Follicular stromal cells and lymphocyte homing to follicles. Immunological reviews 176, 181–193 (2000). [PubMed: 11043777]
34. Green JA et al. The sphingosine 1-phosphate receptor S1P(2) maintains the homeostasis of germinal center B cells and promotes niche confinement. Nat Immunol 12, 672–680 (2011). [PubMed: 21642988]
35. Gatto D, Paus D, Basten A, Mackay CR & Brink R Guidance of B cells by the orphan G protein-coupled receptor EBI2 shapes humoral immune responses. Immunity 31, 259–269 (2009). [PubMed: 19615922]
36. Zhao R et al. A GPR174-CCL21 module imparts sexual dimorphism to humoral immunity. Nature 577, 416–420 (2020). [PubMed: 31875850]
37. Lu P, Shih C & Qi H Ephrin B1-mediated repulsion and signaling control germinal center T cell territoriality and function. Science 356, eaai9264 (2017). [PubMed: 28408722]
38. Pae J et al. Cyclin D3 drives inertial cell cycling in dark zone germinal center B cells. J Exp Med 218, jem.20201699 (2021).
39. Subramanian A et al. Gene set enrichment analysis: a knowledge-based approach for interpreting genome-wide expression profiles. Proc Natl Acad Sci U S A 102, 15545–15550 (2005). [PubMed: 16199517]
40. Kitamura D, Roes J, Kuhn R & Rajewsky K A B cell-deficient mouse by targeted disruption of the membrane exon of the immunoglobulin mu chain gene. Nature 350, 423–426 (1991). [PubMed: 1901381]
41. Ahearn JM et al. Disruption of the Cr2 locus results in a reduction in B-1a cells and in an impaired B cell response to T-dependent antigen. Immunity 4, 251–262 (1996). [PubMed: 8624815]
42. Sivasankar B et al. CD59a deficient mice display reduced B cell activity and antibody production in response to T-dependent antigens. Mol Immunol 44, 2978–2987 (2007). [PubMed: 17296227]
43. Wiede F et al. CCR6 is transiently upregulated on B cells after activation and modulates the germinal center reaction in the mouse. Immunol Cell Biol 91, 335–339 (2013). [PubMed: 23588497]
44. Suan D et al. CCR6 Defines Memory B Cell Precursors in Mouse and Human Germinal Centers, Revealing Light-Zone Location and Predominant Low Antigen Affinity. Immunity 47, 1142–1153 e1144 (2017). [PubMed: 29262350]
45. Carroll MC & Isenman DE Regulation of humoral immunity by complement. Immunity 37, 199–207 (2012). [PubMed: 22921118]
46. Paiano J et al. Follicular B2 Cell Activation and Class Switch Recombination Depend on Autocrine C3ar1/C5ar1 Signaling in B2 Cells. J Immunol 203, 379–388 (2019). [PubMed: 31217324]
47. Dernstedt A et al. Regulation of Decay Accelerating Factor Primes Human Germinal Center B Cells for Phagocytosis. Frontiers in immunology 11, 599647 (2020). [PubMed: 33469456]
48. Biram A, Davidzohn N & Shulman Z T cell interactions with B cells during germinal center formation, a three-step model. Immunological reviews 288, 37–48 (2019). [PubMed: 30874355]
49. Wu YL & Rada C Molecular fine-tuning of affinity maturation in germinal centers. J Clin Invest 126, 32–34 (2016). [PubMed: 26657856]

50. Arbore G et al. T helper 1 immunity requires complement-driven NLRP3 inflammasome activity in CD4(+) T cells. Science 352, aad1210 (2016).
51. Liszewski MK et al. Intracellular complement activation sustains T cell homeostasis and mediates effector differentiation. Immunity 39, 1143–1157 (2013). [PubMed: 24315997]
52. West EE, Afzali B & Kemper C Unexpected Roles for Intracellular Complement in the Regulation of Th1 Responses. Adv Immunol 138, 35–70 (2018). [PubMed: 29731006]
53. Rossbacher J & Shlomchik MJ The B cell receptor itself can activate complement to provide the complement receptor 1/2 ligand required to enhance B cell immune responses in vivo. J Exp Med 198, 591–602 (2003). [PubMed: 12925675]
54. Bird L Switch to antitumour B cells. Nat Rev Immunol 20, 274–275 (2020).
55. Lu Y et al. Complement Signals Determine Opposite Effects of B Cells in Chemotherapy-Induced Immunity. Cell 180, 1081–1097 e1024 (2020). [PubMed: 32142650]
56. Heng TS, Painter MW & Immunological Genome Project C. The Immunological Genome Project: networks of gene expression in immune cells. Nat Immunol 9, 1091–1094 (2008). [PubMed: 18800157]
57. Zhang J et al. Disruption of KMT2D perturbs germinal center B cell development and promotes lymphomagenesis. Nat Med 21, 1190–1198 (2015). [PubMed: 26366712]
58. Zhang M et al. The role of natural IgM in myocardial ischemia-reperfusion injury. J Mol Cell Cardiol 41, 62–67 (2006). [PubMed: 16781728]
59. Llaudo I et al. C5aR1 regulates migration of suppressive myeloid cells required for costimulatory blockade-induced murine allograft survival. Am J Transplant 19, 633–645 (2019). [PubMed: 30106232]
60. Hovingh ES, van den Broek B & Jongerius I Hijacking Complement Regulatory Proteins for Bacterial Immune Evasion. Front Microbiol 7, 2004 (2016). [PubMed: 28066340]
61. Mashiko D et al. Generation of mutant mice by pronuclear injection of circular plasmid expressing Cas9 and single guided RNA. Scientific reports 3, 3355 (2013). [PubMed: 24284873]
62. Kwan WH et al. Antigen-presenting cell-derived complement modulates graft-versus-host disease. J Clin Invest 122, 2234–2238 (2012). [PubMed: 22585573]
63. Le TV, Kim TH & Chaplin DD Intraclonal competition inhibits the formation of high-affinity antibody-secreting cells. J Immunol 181, 6027–6037 (2008). [PubMed: 18941192]
64. Phan RT & Dalla-Favera R The BCL6 proto-oncogene suppresses p53 expression in germinal-centre B cells. Nature 432, 635–639 (2004). [PubMed: 15577913]
65. Gitlin AD, Shulman Z & Nussenzweig MC Clonal selection in the germinal centre by regulated proliferation and hypermutation. Nature 509, 637–640 (2014). [PubMed: 24805232]
66. Jacob J & Kelsoe G In situ studies of the primary immune response to (4-hydroxy-3-nitrophenyl)acetyl. II. A common clonal origin for periarteriolar lymphoid sheath-associated foci and germinal centers. J Exp Med 176, 679–687 (1992). [PubMed: 1512536]
67. Lefranc MP et al. IMGT, the international ImMunoGeneTics information system. Nucleic Acids Res 37, D1006–1012 (2009). [PubMed: 18978023]
68. Alamyar E, Duroux P, Lefranc MP & Giudicelli V IMGT((R)) tools for the nucleotide analysis of immunoglobulin (IG) and T cell receptor (TR) V-(D)-J repertoires, polymorphisms, and IG mutations: IMGT/V-QUEST and IMGT/HighV-QUEST for NGS. Methods Mol Biol 882, 569–604 (2012). [PubMed: 22665256]
69. MacCarthy T et al. V-region mutation in vitro, in vivo, and in silico reveal the importance of the enzymatic properties of AID and the sequence environment. Proc Natl Acad Sci U S A 106, 8629–8634 (2009). [PubMed: 19443686]
70. Kim D, Langmead B & Salzberg SL HISAT: a fast spliced aligner with low memory requirements. Nat Methods 12, 357–360 (2015). [PubMed: 25751142]
71. Liao Y, Smyth GK & Shi W featureCounts: an efficient general purpose program for assigning sequence reads to genomic features. Bioinformatics 30, 923–930 (2014). [PubMed: 24227677]
72. Love MI, Huber W & Anders S Moderated estimation of fold change and dispersion for RNA-seq data with DESeq2. Genome Biol 15, 550 (2014). [PubMed: 25516281]
73. Reich M et al. GenePattern 2.0. Nat Genet 38, 500–501 (2006). [PubMed: 16642009]

74. Faul F, Erdfelder E, Lang AG & Buchner A G*Power 3: a flexible statistical power analysis program for the social, behavioral, and biomedical sciences. Behav Res Methods 39, 175–191 (2007) [PubMed: 17695343]

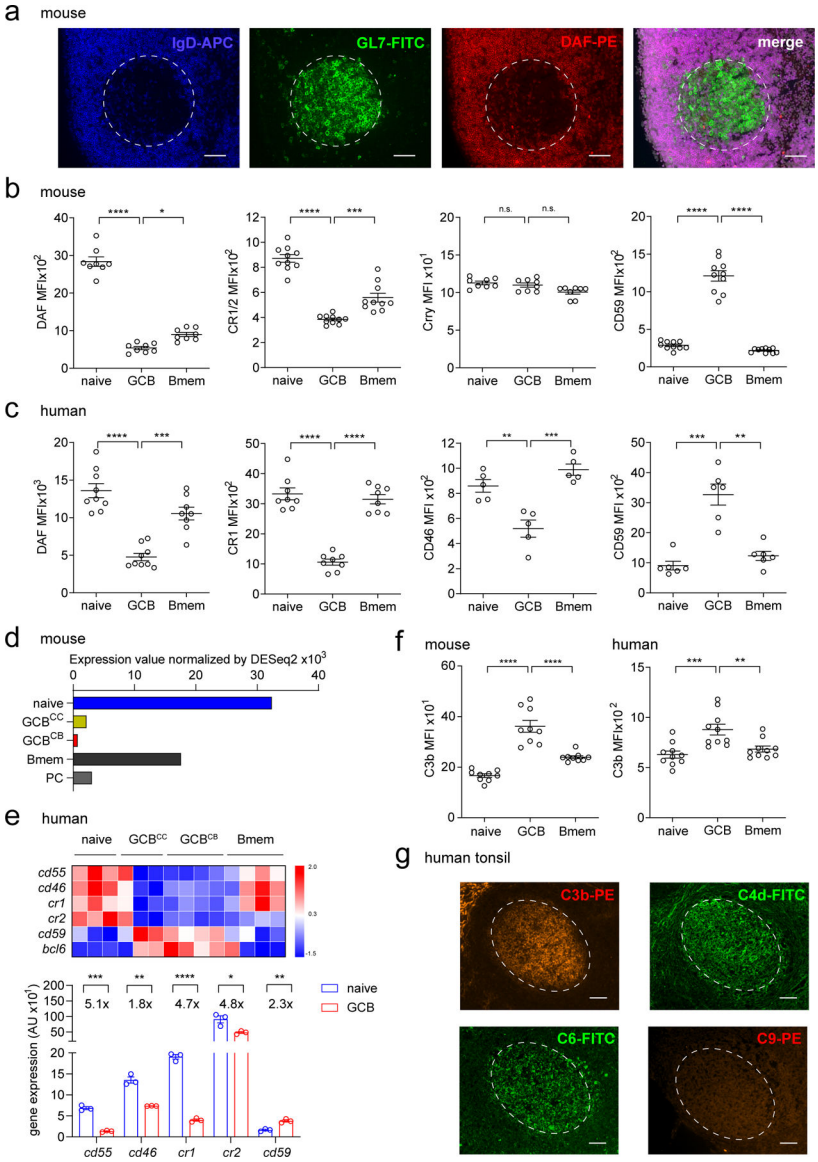

Figure 1. GC B cells downregulate expression of DAF (CD55) and other C3/C4 convertase inhibitors within the RCA

a. Representative (10 different experiments) immunofluorescence (IF) analysis of a splenic GC from a WT C57BL/6 mouse, d10 post immunization with NP-KLH; stained for IgD (naïve B cells), GL7 (GC B cells) and DAF. Scale bar, 50 μm. **b-c**. Flow cytometry analysis of mouse (**b**) and human (**c**) B cell subsets stained for DAF, CR1/2, Crry (mouse), CD46 (human) and CD59, as indicated. Each dot represents a biological replicate. Gating strategy in Extended data Fig 1a–b. **d**. DAF mRNA expression in murine B cell subsets. Data extracted from the Immgen database [56]. **e.** Heat map (top, microarray) and transcript number (bottom, RNAseq, inset numbers: fold change) of human complement regulator expression; data source: GSE2350 (heatmap) and GSE139833 (bar graph). **f.** Flow cytometry analysis of mouse (left) and human (right) B cell subsets stained for C3b. Each dot represents one biological replicate. **g.** Representative IF analysis of human tonsil GC staining for C3b, C4d, C6 but not C9 (positive control shown in Extended data Fig 1h). Scale bar, 50 μm. **a** and **g**

representative of >3 experiments. Data are presented as MFI +/− SEM, *p<0.05, **p<0.01, ***p<0.005, ****p<0.001 by one-way ANOVA with Bonferroni post-test (**b-c**, **f**), or mean +/− SEM, Students t-test for **e** (bottom).

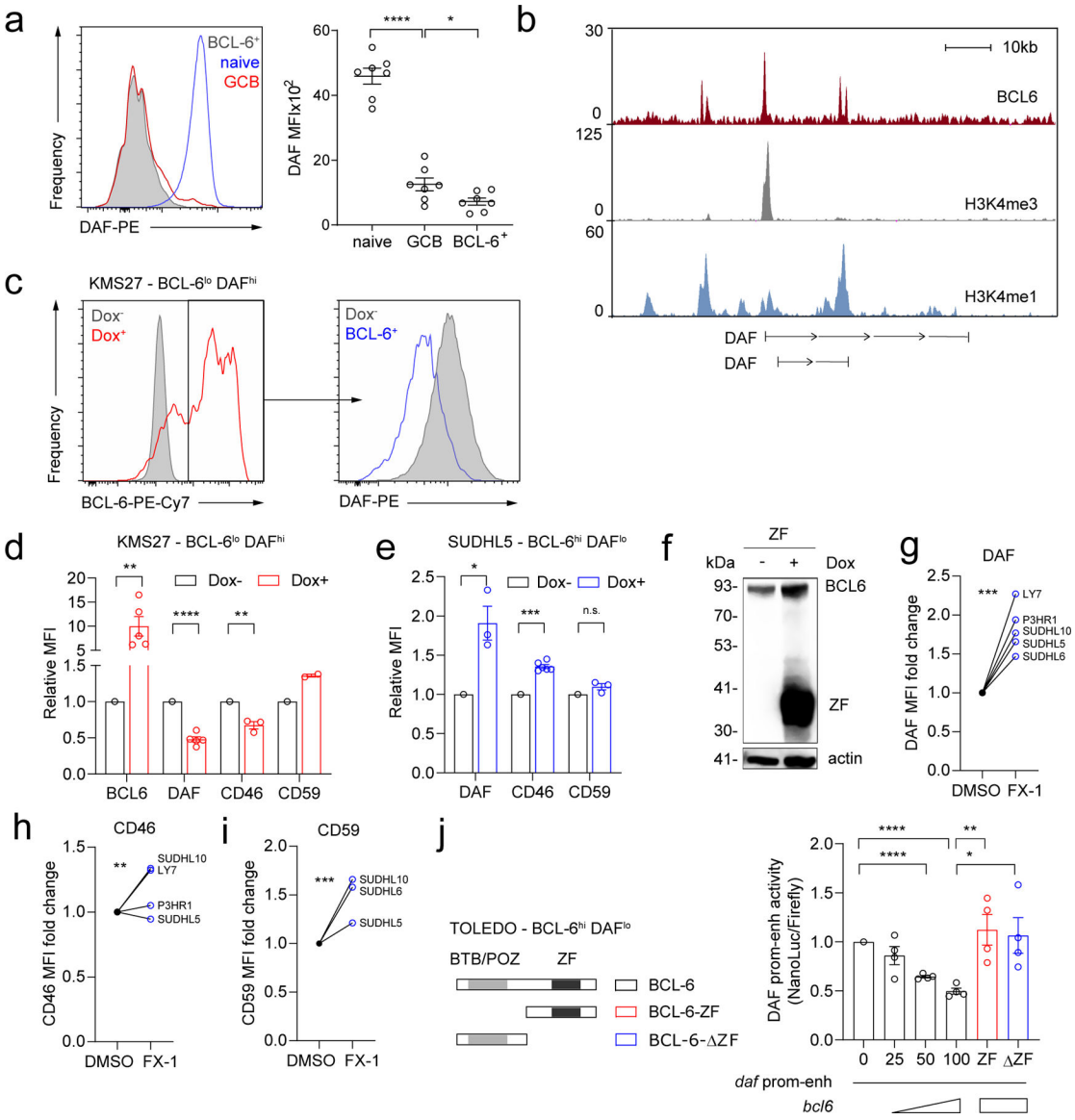

Figure 2. BCL-6 transcriptionally represses DAF expression in GC B cells.

a. Representative histogram (left) and quantified results (right) of DAF (CD55) and Bcl-6 on BCL-6-YFP^{+} B cells, d3 post-immunization (gating strategy, Extended data Fig 2b); mean ±SEM. **b.** ChIPseq analysis of human GC B cells (tonsil) showing distribution of BCL-6, H3K4Me1 and H3K4Me3 marks at the *CD55* gene (from GSE68349, GSE67494)[18, 57]. **c-d.** Representative histograms for BCL-6 (**c**, left) and DAF (**c**, right) with quantification (**d**) for BCL-6, DAF, CD46 and CD59 on KMS27 (multiple myeloma) cells following BCL-6 overexpression (n=5 for BCL-6 and DAF, n=3 for CD46; n=2 for CD59). **e-f**. Quantified changes in DAF, CD46 and CD59 expression on SUDHL5 DLBCL B-lymphoma cells (**e**), (DAF & CD59, n=3; CD46, n=6); following transfection with a dominant negative (ZF) BCL-6 (**f**, representative immunoblot). The anti-BCL-6 antibody recognizes a region present in the ZF domain of this protein (BCL-6, full-length protein) **g-i.** Fold change in surface expression of DAF (**g**), CD46 (**h**) and CD59 (**i**) by flow cytometry 24h after addition of

BCL-6 inhibitor FX1 (50 mM), or DMSO control. FX1 significantly upregulated DAF in 5 cell lines (SUDHL5, n=6; SUDHL6, n=4; SUDHL10, n=8; P3HR1, n=2; OCI-LY7, n=3). p value is a summary of all replicates for all lines. FX1 upregulated CD46 in OCI-LY7, n=1 and SUDHL10, n=2 (p value shown for these 3 combined replicates) without effect in SUDHL5, n=2 and P3HR1 n=2 (p value for these combined replicates: ns). FX1 upregulated CD59 in 3/3 lines (SUDHL5, n=3; SUDHL6, n=4; SUDHL10 n=3). p value is shown for these 10 combined replicates from the 3 cell lines. Data are presented as normalized to DMSO levels for each experiment **j**. left: construct schematics for BCL-6, BCL-6 DNA binding domain ZF and BCL-6 that lacks DNA binding domain delta ZF. right: quantified luciferase signal under each condition, For all panels, data are presented as mean values +/− SEM, *p<0.05, **p<0.01, ***p<0.005, ****p<0.001 by ANOVA with Bonferroni post-test (**a, j**) unpaired t-test, two-tailed (**a,d-e**) or paired t-test, two-tailed (**g**). ns, not significant.

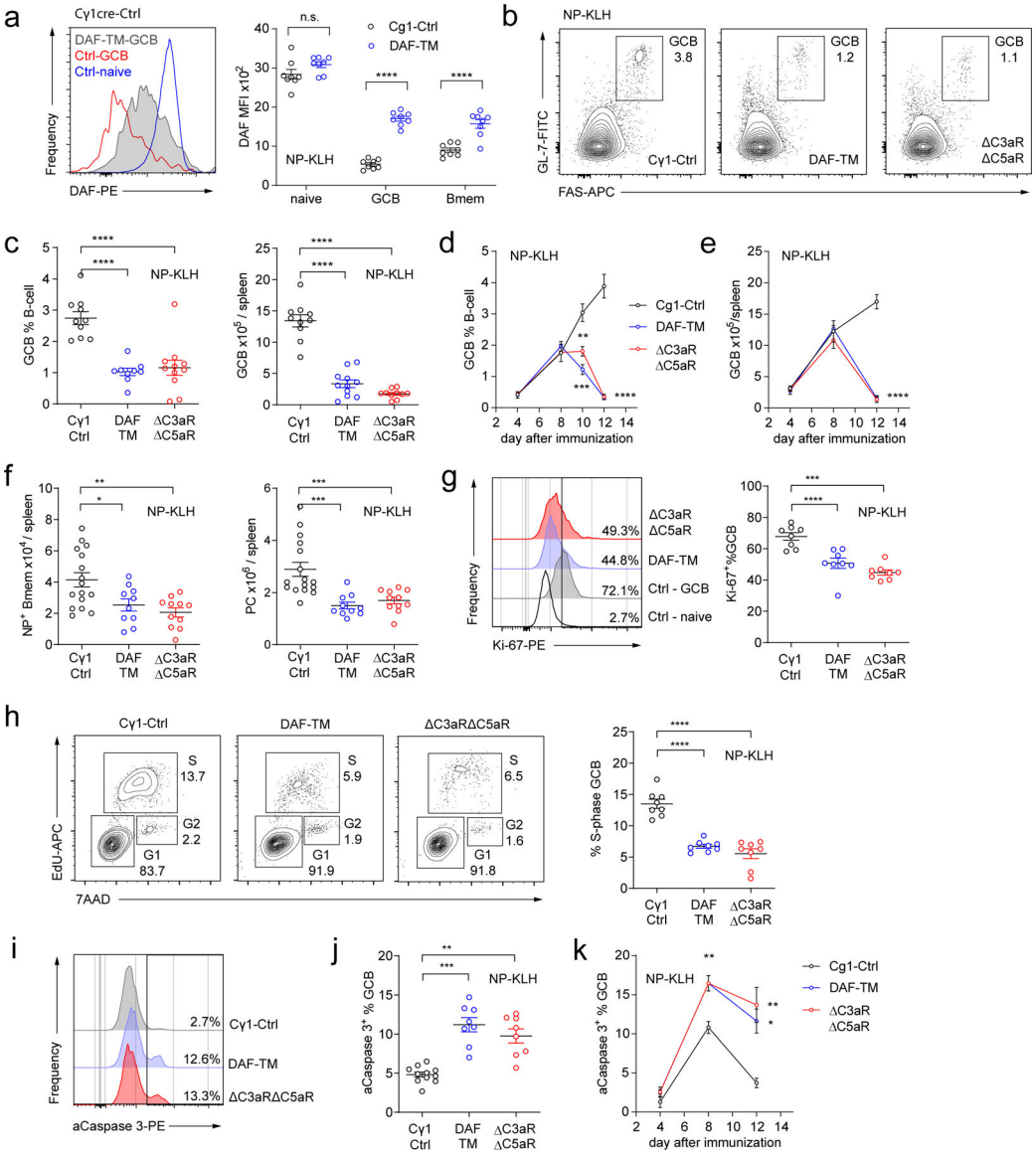

Figure 3. Transgenic DAF overexpression or absence of C3ar1/C5ar1 on GC B cells aborts GC formation.

a. Representative histogram (left) and quantitation (right) of DAF (CD55) expression on B cell subsets from DAF-TM$^{C\gamma1}$ (blue) and *Cγ1*-Cre$^{+/-}$ (Ctrl, black) mice d12 post-immunization with NP-KLH**. b-k**. All experiments and analyses were performed on groups of d10–12 NP-KLH-immunized, DAF-TM$^{C\gamma1}$ (DAF TM), Δ*C3ar1*/*C5ar1*$^{C\gamma1}$ (ΔC3aRΔC5aR) and control *Cγ1*-Cre$^{+/-}$ (Cγ1 Ctrl) mice**. b-c**. Representative contour plots (**b**) and quantification (**c**) of d12 percentage (left) and total (right) splenic GC B cells. **d-e**. Kinetic analysis of relative percentages (**d**) and total (**e**) splenic GC B cells. **f**. Quantification of d12 splenic memory B cell (left, B220^{+}IgD^{-}GL7^{-}Fas^{-}CD38^{+}NP^{+} Bmem), and plasma cells (right, CD19^{+}B220^{dim}CD138^{+}PC) See also Extended data. Fig 4i–k. **g**. Representative histograms (left) and quantification of % Ki67^{+} (right) GC B cells. **h**. Representative contour plots (left) and quantitation (right) of EdU incorporation and DNA content (7AAD) by GC B cells. **i-k**. Representative histograms (**i**, left), d12 quantification (**j**); and kinetics (**k,** n=4 per

time point for each genotype) of activated caspase 3^+ (aCaspase3) in splenic GC B cells; Data are presented as mean values +/− SEM, *p<0.05,**p<0.01, ***p<0.005, ****p<0.001, by ANOVA with Bonferroni post-test (for kinetics in **d-e, k**, 3 genotypes were compared at each time point), n.s., not significant. Each dot represents a biological replicate.

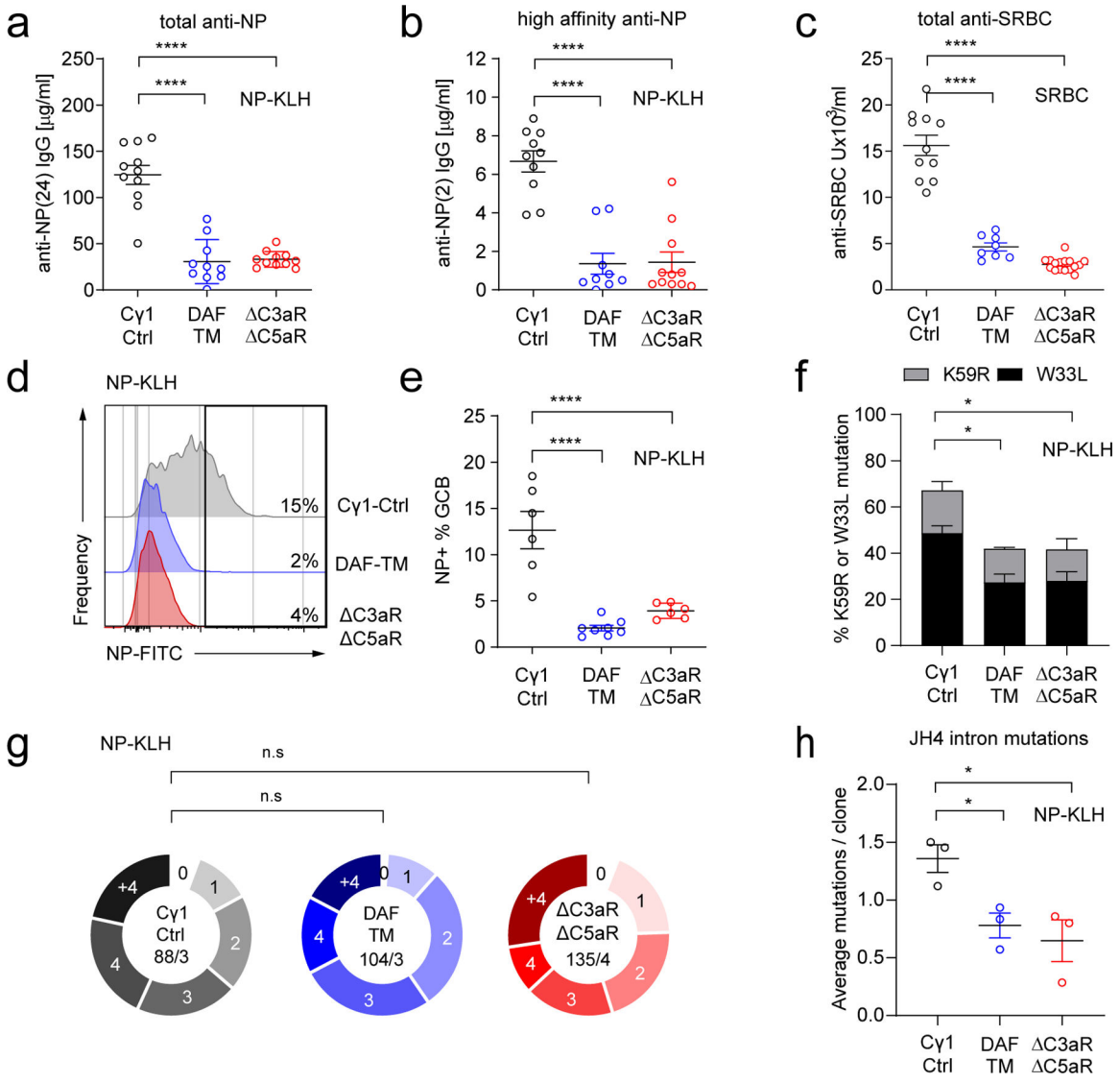

Figure 4. Transgenic DAF overexpression or absence of C3ar1/C5ar1 on GC B cells limits affinity maturation.

a-b. Serum ELISA for total anti-NP(24) (**a**) and high affinity anti-NP(2) (**b**) antibodies from d12 immunized mice. **c.** Quantified serum anti-SRBC antibodies from d12 SRBC-immunized DAF-TM$^{C\gamma1}$ (DAF TM), Δ*C3ar1*/*C5ar1*$^{C\gamma1}$ (ΔC3aRΔC5aR) and control *Cγ1*-Cre$^{+/-}$ (Cγ1 Ctrl) mice. **d-e**. Representative flow histogram (**d**) and quantification (**e**) of d12 splenic NP-specific GC B cell from DAF-TM$^{C\gamma1}$, Δ*C3ar1*/*C5ar1*$^{C\gamma1}$ and *Cγ1*-Cre$^{+/-}$ mice. **f-g.** Quantified frequencies of high affinity W33L^{+} (±K59R, or K59R alone) lambda BCRs (**f**) with clone distribution (**g**) based on number of somatic mutations (0 to >4). The number of clones and animals analyzed per genotype are indicated in the center of each graph. **h.** Quantification of mutation frequency per 100bp in J_{H4} segments, plotted by genotype (n=3 animals per group); Data are presented as mean values +/− SEM, *p<0.05,**p<0.01, ***p<0.005, ****p<0.001 by ANOVA with Bonferroni post-test (**a-c**, **e** and **h**), Fisher's exact test (**f**), Chi-Square (**g**), n.s. not significant. Each dot represents a biological replicate. See also Supplementary Table 1.

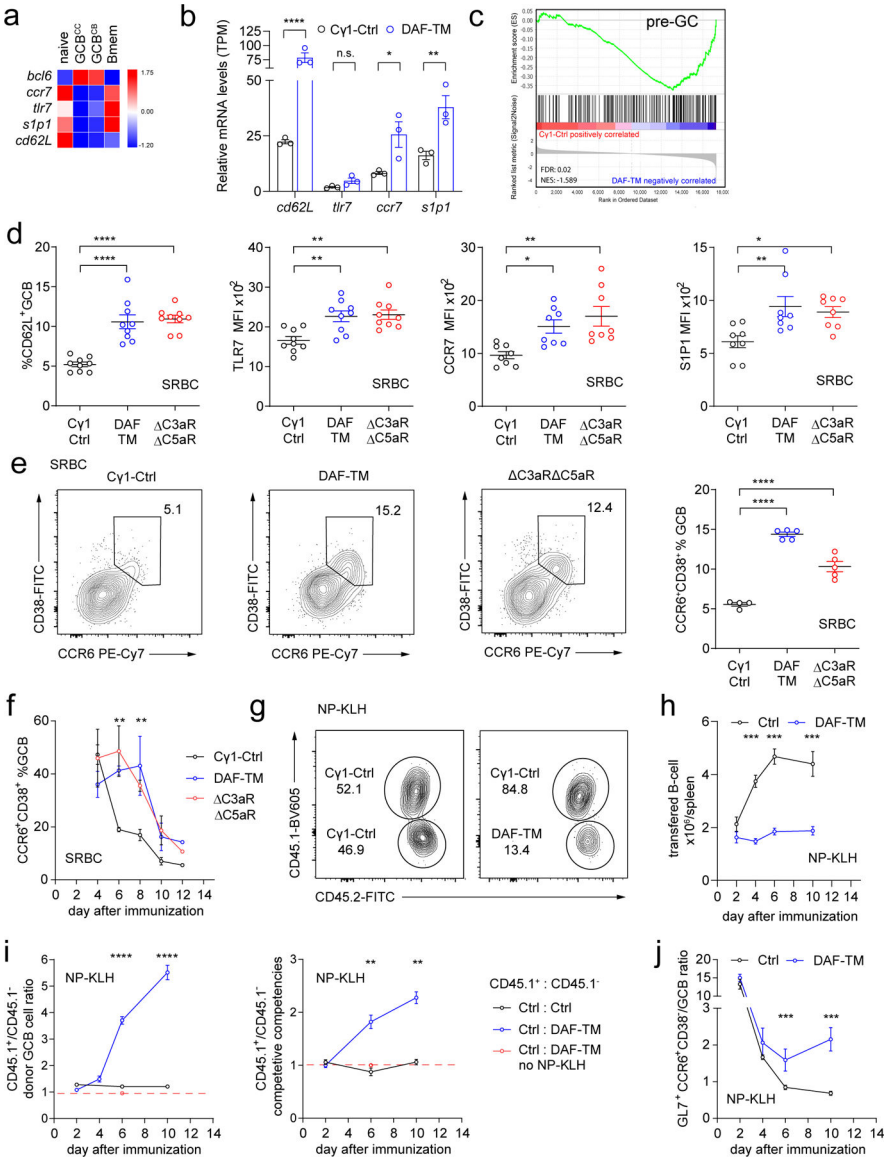

Figure 5. Defective expansion, delayed maturation and reduced competitive competencies of DAF-TM$^{C\gamma1}$, Δ*C3ar1*/*C5ar1*$^{C\gamma1}$ B cells during GC responses

a. Heat map depicting relative mRNA expression levels (row normalization) of selected genes in murine B cell subsets (source: ImmGen database). **b.** Relative mRNA expression of the genes shown in (**a**) in GC-B cells isolated from SRBC-immunized DAF-TM$^{C\gamma1}$ and *Cγ1*-Cre$^{+/-}$ mice on d10 (RNA-seq; Transcripts per million, TPM). p-values estimated using DESeq2. **c.** Enrichment plot depicting gene set distribution of a pre-GC gene signature in DAF-TM$^{C\gamma1}$ vs. *Cγ1*-Cre$^{+/-}$ GC B cells (GSE12845_PRE_GC_VS_DARKZONE_GC_TONSIL_BCELL_UP). **d.** Quantified percentage of CD62L^{+} GC B cells; and surface expression levels of TLR7, CCR7 and S1P1 (MFI, as indicated) on d10 SRBC-immunized GL7^{+}Fas^{+} GC B cells from DAF-TM$^{C\gamma1}$ (DAF TM), Δ*C3ar1*/*C5ar1*$^{C\gamma1}$ (ΔC3aRΔC5aR) and control *Cγ1*-Cre$^{+/-}$ (Cγ1 Ctrl) mice (representative plots shown in Extended data Fig 7b) **e-f.** Representative contour plots (**e**, left 3 panels), relative frequency (**e**, right panel, d10) and (**f**) kinetics of CCR6^{+}CD38^{+}

expressing GC B cells in SRBC-immunized DAF-TM$^{C\gamma1}$, Δ*C3ar1*/*C5ar1*$^{C\gamma1}$ and *Cγ1*-Cre $^{+/-}$ mice. **g-i**. In vivo competition of control (CD45.1/2 or CD45.2) and DAF-TM^{+} (CD45.2) B1–8^{hi} cells in NP-KLH immunized CD45.1 hosts. **g.** representative d6 flow cytometry plots following co-transfer of CD45.2 control vs. CD45.1/2 control B1–8^{hi} cells (left), or CD45.2 DAF-TM^{+} vs CD45.1/2 control B1–8^{hi} cells (right). **h.** kinetics of control vs. DAF-TM^{+} B1–8^{hi} cell expansion in NP-KLH immunized hosts. **i**. kinetic analysis of control vs. DAF-TM^{+} B1–8^{hi} GC B cell ratios (left) and normalized competitive competency indices (right) for CD45.1/2 control to CD45.2 DAF-TM^{+} B1–8^{hi} cells (blue) or CD45.1/2 control: CD45.2 ctrl B1–8^{hi} cells (black) in NP-KLH immunized hosts, and CD45.1/2 control: CD45.2 control B1–8^{hi} cells in unimmunized hosts (red). **j.** kinetics of ratios of %GL7^{+}CCR6^{+}CD38^{+} : GL7^{+}Fas^{+} GC B1–8^{hi} cells of DAF-TM^{+} (blue) or control B1–8^{hi} cells (black). Data are presented as mean values +/− SEM, *p<0.05, **p<0.01, ****p<0.001 by ANOVA with Bonferroni post-test (**c-j**, for kinetics in **f-j**, 3 genotypes were compared at each time point) or unpaired Student's t-test (**b**). Each dot represents a biological replicate.

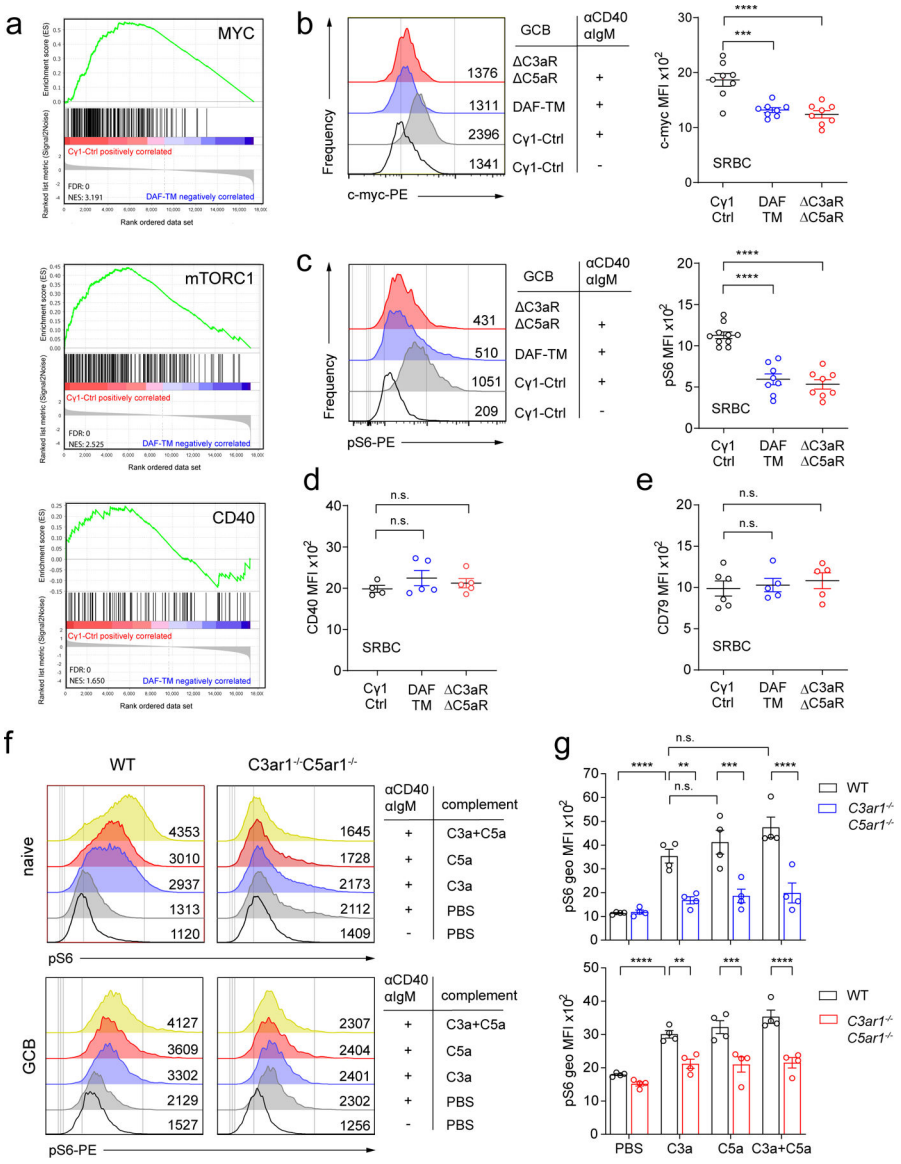

Figure 6. DAF-TM and absent C3aR/C5aR signaling on GCB cells reduces signals required for positive selection independent of CD40.

a. GSEA enrichment plots for selected gene sets in DAF-TM$^{C\gamma1}$ vs. *Cγ1*-Cre$^{+/-}$ mice. NES, normalized enrichment score; FDR, false discovery rate. **b-c**. Representative histograms (left) and quantification (right) for MYC (**b**) and phosphorylated S6 ribosomal protein (pS6, **c**) in d10 GC B cells isolated 4h after *in vivo* stimulation with anti-CD40/IgM F(ab')$_2$ (see Extended data Fig 8b–d for controls). **d-e.** quantified CD40 (MFI, **d**) and CD79 (Igα/Igβ, **e**) expression on GC B cells, d10 post-SRBC immunization in DAF-TM$^{C\gamma1}$ (DAF TM), Δ*C3ar1*/*C5ar1*$^{C\gamma1}$ (ΔC3aRΔC5aR) and control *Cγ1*-Cre$^{+/-}$ (Cγ1 Ctrl) mice. (**f-g**) Representative pS6 flow histograms (**f**) and quantified results (**g**) of naïve (top) and GC B cells (bottom) from WT or germline *C3ar1*$^{-/-}$*C5ar1*$^{-/-}$ mice, stimulated *in vitro* for 20 min with subthreshold amounts of anti-CD40/IgM F(ab')$_2$ ± recombinant C3a, C5a proteins, as indicated (see Extended data Fig 8h). Data are presented as MFI +/− SEM n=5–8/group.

*p<0.05, **p<0.01, ***p<0.005, ****p<0.001 by ANOVA with Bonferroni post-test (**b-e, g**). Each dot represents a biological replicate. n.s., not significant.